

# TECTONIC EVOLUTION OF AN EARLY CRYOGENIAN LATE- MAGMATIC BASIN IN CENTRAL MADAGASCAR

Costa, R.L.<sup>1</sup>, Schmitt, R.S.<sup>1,2\*</sup>, Collins, A.S.<sup>3</sup>, Armistead, S.E.<sup>3,4,5</sup>, Gomes,  
I.V.<sup>1,2</sup>, Archibald, D.B.<sup>6</sup>, Razakamanana, T.<sup>7</sup>

<sup>1</sup>Programa de Pós-graduação em Geologia, Universidade Federal do Rio de Janeiro (PPGL/UFRJ), CEP 21941-916, Rio de Janeiro, Brazil – [raisa.ric23@gmail.com](mailto:raisa.ric23@gmail.com)

<sup>2</sup>Departamento de Geologia, Instituto de Geociências, Universidade Federal do Rio de Janeiro, Av. Athos da Silveira Ramos, 274/ bloco J, sala 022 - Cidade Universitária – Rio de Janeiro – RJ – CEP 21941-909 – Brazil – [schmitt@geologia.ufrj.br](mailto:schmitt@geologia.ufrj.br)

<sup>3</sup>Tectonics and Earth Systems (TES), Mawson Geoscience Centre, Department of Earth Sciences, The University of Adelaide, SA 5005, Australia – [alan.collins@adelaide.edu.au](mailto:alan.collins@adelaide.edu.au) (@geoAlanC)

<sup>4</sup>Geological Survey of Canada, 601 Booth Street, Ottawa, ON, K1A 0E9 Canada – [sarmistead@laurentian.ca](mailto:sarmistead@laurentian.ca) (@geoSheree)

<sup>5</sup>Mineral Exploration Research Centre, Harquail School of Earth Sciences, Laurentian University, Sudbury, ON, P3E 2C6 Canada

<sup>6</sup>Department of Earth Sciences, St. Francis Xavier University, Physical Sciences Complex, 5009 Chapel Square, Antigonish, NS, Canada, B2G 2W5 – [darchiba@stfx.ca](mailto:darchiba@stfx.ca) (@darchibald12)

<sup>7</sup>Département des Sciences de la Terre, Université de Toliara, Toliara, Madagascar – [razakamananat@yahoo.fr](mailto:razakamananat@yahoo.fr)

\* Corresponding author at: Departamento de Geologia, Instituto de Geociências, Universidade Federal do Rio de Janeiro, Av. Athos da Silveira Ramos, 274/ bloco J, sala 022 - Cidade Universitária – Rio de Janeiro – RJ – CEP 21941-909 – Brazil . Tel.: +55 21 996388859 - E-mail: [schmitt@geologia.ufrj.br](mailto:schmitt@geologia.ufrj.br)

---

This manuscript is not published and is under review in the Journal of African Earth Sciences. Please note that subsequent versions of this manuscript will have slightly different content. If accepted, the final version of this manuscript will be available via the 'Peer-reviewed Publication DOI' link on the right-hand side of this webpage.

\*corresponding author: Renata da Silva Schmitt – [schmitt@geologia.ufrj.br](mailto:schmitt@geologia.ufrj.br)

---

1 **Highlights:**

- 2 • Early Cryogenian basin with volcanoclastic contribution in Central
- 3 Madagascar
- 4 • Three distinct tectonic models for Late Tonian-Early Cryogenian
- 5 • Extensional intracontinental magmatic setting related to an outboard
- 6 subduction
- 7 • A transform continental setting resolves the tectonic Cryogenian paucity
- 8 • Continental collision dated with 550 Ma metamorphic rims on zircons

9 **ABSTRACT**

10 Central and southern Madagascar comprise a number of distinctive Archaean  
11 crustal blocks (the Antongil-Masora and Antananarivo domains) overlain by  
12 Proterozoic supracrustal sequences, preserved in the East African Orogen. Here, we  
13 present U–Pb and Lu–Hf isotopic data for two supracrustal units from detrital and  
14 metamorphic zircon grains. The lower sequence is comprised of quartzite and calc-  
15 silicate units with a major Palaeoproterozoic detrital zircon source and a minor  
16 Archaean contribution with a maximum depositional age of ca. 1780 Ma. This  
17 sequence reflects a stable shelf sedimentation within the Antananarivo Domain and  
18 is correlated with the Itremo Group. U–Pb and Hf data are equivocal in determining  
19 the direct sources for the Archaean and early Palaeoproterozoic detrital zircon grains.  
20 However, the abundant ca. 2.3-1.8 Ga detrital grains are correlative with the Congo-  
21 Tanzania-Bangweulu Block and as these are close to the inferred age of the Itremo  
22 Basin, these are interpreted to be single cycle detritus. This implies that the Congo-  
23 Tanzania-Bangweulu craton was close to central Madagascar at ca. 1.8-1.6 Ga and  
24 the lower sequence would correspond to an originally contiguous late  
25 Palaeoproterozoic to early Mesoproterozoic sedimentary basin across central

26 Madagascar. The upper metasedimentary unit has contrasting detrital sources and  
27 is represented mostly by biotite-plagioclase paragneiss, with an inferred psammitic  
28 protolith interleaved with volcanic/subvolcanic andesitic/rhyolitic dikes. The  
29 predominant Tonian-aged population (ca. 860-710 Ma) are igneous zircon grains  
30 with  $\epsilon_{\text{Hf}}(t)$  values varying from -15.1 to -29.2 and  $T_{\text{DM}}$  Hf model ages between ca. 3.4  
31 and 2.6 Ga. These grains were derived from the ca. 850-750 Ma Imorona-Itsindro  
32 magmatic suite. Their Neoarchaeon-Palaeoproterozoic cores are interpreted as  
33 xenocrysts, reinforcing that the Imorona-Itsindro magmatism has a prominent  
34 continental reworking component. The probable tectonic setting for this Early  
35 Cryogenian sedimentary basin would represent a transition from an intra-arc to an  
36 intracontinental setting related to an outboard subduction, partially jammed at ca. 710  
37 Ma due to the subduction of a ridge-transform system. The analogue would be the  
38 western US, where the Basin and Range region corresponds to a wide rift associated  
39 with a major mantle thermal anomaly. The absence of geological units and structures  
40 between ca. 720 and 635 Ma in central Madagascar corroborate with this model for  
41 a transition to a transform continental setting. The pre-Gondwana amalgamation  
42 convergence in the Ediacaran-Cambrian, that deformed and metamorphosed all  
43 units in central Madagascar units, is accounted for by ca. 550 Ma metamorphic rims  
44 on zircon grains from the quartzites in the Itremo Group.

45

#### 46 **Keywords**

47 Imorona-Itsindro Suite, late-magmatic continental basin, Cryogenian, detrital  
48 zircon, Central Gondwana

49

## 50 **1. Introduction**

51 The East African Orogen (EAO) involves a collection of Neoproterozoic  
52 microcontinents and arc terranes lodged between older cratonic domains that  
53 coalesced during the final assembly of supercontinent Gondwana (Collins and  
54 Pisarevsky, 2005; Schmitt et al., 2018), extending from the Arabian Peninsula along  
55 eastern Africa, southern India, Sri Lanka and into Antarctica (Grantham et al., 2011;  
56 Jacobs and Thomas, 2004; Jacobs et al., 1998). This orogenic system resulted in the  
57 closure of the Mozambique Ocean between the eastern and western Gondwana  
58 blocks during the Neoproterozoic-Cambrian transition (Merdith et al., 2017; Tucker et  
59 al., 2014). The record of convergence between the Greater Dharwar Craton and the  
60 Congo/Tanzania/Bangweulu blocks (southern India and eastern Africa, respectively),  
61 is preserved within the Malagasy basement (Fig. 1a; Collins, 2006; Stern, 1994,  
62 2002).

63 This basement in central and southern Madagascar comprise a number of  
64 distinctive Archaean crustal blocks (Antongil-Masora and Antananarivo domains) that  
65 are overlain by several Proterozoic sedimentary and volcano-sedimentary sequences  
66 (Fig. 1b), metamorphosed during the Neoproterozoic-Cambrian (De Waele et al.,  
67 2011; Tucker et al., 2007). The metasedimentary units include the Itremo,  
68 Ikalamavony, Ambatolampy, Maha, Manampotsy, Sahantaha, Andrarona and Molo  
69 groups (Bauer et al., 2011, Archibald et al., 2015; Cox et al., 2004a; De Waele et al.,  
70 2011). These supracrustal rocks record hundreds of millions of years of convergent  
71 tectonics, as pre-, syn-, late- and post-tectonic basins.

72 Although these metasedimentary sequences have U–Pb provenance studies  
73 (Cox et al., 1998, 2004a; De Waele et al., 2011; Boger et al. 2014), many questions  
74 remain regarding the relationship of these sedimentary and volcanic rocks with two

75 well described magmatic arcs: the Dabolava Suite that formed on a juvenile intra-  
76 oceanic arc at ca.1000 Ma (Archibald, et al., 2018; CGS, 2009a, 2009b; Tucker et al.,  
77 2007), and the Imorona-Itsindro Suite that formed in a continental arc setting at ca.  
78 850-750 Ma (Archibald et al., 2016, 2017; Boger et al. 2014, 2015; Handke et al.,  
79 1999). In addition, the period between ca. 700 Ma, the age of the last preserved pre-  
80 collisional magmatic unit, and ca. 575 Ma, the age of the main metamorphic and  
81 deformational event related to the EAO within Madagascar, is still poorly understood  
82 in terms of the tectonic regime.

83 Here, we present new geological and geochronological data for two  
84 supracrustal units from the Ikalamavony region in the west-central part of  
85 Madagascar, including U–Pb geochronology and Lu-Hf isotopes on detrital and  
86 metamorphic zircon grains. We examine the existence of an early Cryogenian  
87 sedimentary basin with an important volcanoclastic contribution that developed  
88 coevally with Imorona-Itsindro suite magmatic activity. We also investigate a pre-  
89 Neoproterozoic sedimentary basin that is tectonically juxtaposed with the Early  
90 Cryogenian sequence.

91

92

## 93 **2. Tectonic setting and geology**

94 Precambrian tectonic domains make up the Malagasy basement (Fig. 1). The  
95 oldest blocks, the Antongil and Masora cratons, are located on the eastern coast and  
96 consist of Paleoarchaeon to Mesoarchaeon ortho- and paragneisses (ca. 3330-3140  
97 Ma) with Neoarchaeon granitic and metasedimentary rocks (ca. 2540-2500 Ma; BGS,  
98 2008; Schofield et al., 2010; Tucker et al., 1999, 2011b). Nonetheless, two key  
99 differences between the cratons are acknowledged. The first is the ensuing magmatic  
100 activity recorded at ca. 2350 Ma and ca. 2150 Ma that occurs only in the Antongil  
101 Craton (Schofield et al., 2010; Bauer et al., 2011). The second is the  
102 Palaeoproterozoic supracrustal unit that overlies the Masora Craton, the so-called  
103 Maha Group (maximum depositional age ca. 1700 Ma), cropping out in the eastern  
104 portion of Madagascar (De Waele et al., 2008, 2011). Additionally, Bauer et al. (2011)  
105 reported a sequence of low-grade Proterozoic sediments overlying the Antongil  
106 Craton (Fig.1a), the Andrarona Group. The basal component of the Andrarona Group,  
107 the Ankavia Formation, has a maximum depositional age of  $2355 \pm 11$  Ma ( $2\sigma$ ), while  
108 the upper formation within this group – the Andratany Formation – has euhedral  
109 zircons of interpreted volcanic origin yielding an age of  $1875 \pm 8$  Ma ( $2\sigma$ ). According  
110 to Tucker et al. (1999, 2014), these rocks in the Antongil and Masora cratons are not  
111 considered to be affected by Neoproterozoic tectonothermal events and they  
112 correlate with the Greater Dharwar Craton, only separating during Gondwana break-  
113 up at ca. 85 Ma (Storey et al., 1995).

114 The central highlands of Madagascar comprise the Antananarivo Domain (Fig.  
115 1b; Collins, 2006; Kröner et al., 2000). It consists of Neoarchaeon stratified gneisses  
116 of the Sofia and Vondrozo groups, to the north and the south, represented by  
117 metasedimentary and metavolcanic rocks, intruded by the granitoids of the Siderian

118 Betsiboka Suite (ca. 2.52–2.49 Ga; BGS-USGS-GLW, 2008; Collins, 2006; Collins  
119 et al., 2003a; Kröner et al., 2000; Roig et al., 2012, Tucker et al., 2014).

120 The Antananarivo cover units Orthogneisses of the Antananarivo Domain are  
121 interleaved with a supracrustal package, the Ambatolampy Group (Figs. 1b and 2),  
122 consisting of graphite-bearing sillimanite ± mica schist/paragneiss with abundant  
123 quartzite beds (BGS-USGS-GLW, 2008). Limited U–Pb geochronology on detrital  
124 zircon was used to suggest a maximum depositional age of  $1056 \pm 54$  Ma; with most  
125 detrital zircon dated between ca. 2740 and ca. 1800 Ma (Figs. 1b and 2; BGS-USGS-  
126 GLW, 2008). In contrast, Archibald et al. (2015) analysed multiple samples and  
127 obtained an age of  $1836 \pm 25$  Ma for the youngest detrital zircon from the  
128 Ambatolampy Group. They proposed that the ca. 1.0 Ga sample, dated previously,  
129 was part of the Manampotsy Group and that the rest of the mapped Ambatolampy  
130 Group is very similar and related to the Itremo Group, forming a contiguous Palaeo-  
131 to early Mesoproterozoic basin (Fig. 1b and 2). The Maha and Sahantaha groups also  
132 overlie Archaean rocks and have comparable detrital zircon ages to the Itremo Group  
133 (Archibald et al., 2015; Cox et al., 2004a; De Waele et al., 2011).

134 The Manampotsy Group, between the Antongil-Masora cratons and the  
135 Antananarivo domain, is a package of supracrustal rocks with pods of mafic-  
136 ultramafic rocks with abundant intrusions of tonalitic to granitic bodies (Fig. 1b - BGS-  
137 USGS-GLW, 2008; Key et al., 2011). The younger population of U–Pb ages on detrital  
138 zircon grains ranges between ca. 840 Ma to ca. 790 Ma but abundant Archaean  
139 grains also occur (Collins et al. 2003a; Tucker et al. 2011b). This indicates that  
140 sedimentary protoliths were deposited from recently formed crustal sources as well  
141 as from the proximal basement. This group has been interpreted as representing  
142 volcanic-arc related sediments, deposited within an active forearc margin basin,

143 representing the Betsimisaraka Suture (Collins et al., 2006; Fig. 1b) (BGS-USGS-  
144 GLW, 2008; Key et al., 2011; Collins et al. 2003b). This unit is also interpreted as  
145 deposited in an intracontinental basin in the Tonian produced by continental extension  
146 lasting more than 80 m.y (Tucker et al., 2011b).

147         The Itremo Group is a sedimentary sequence that overlies the Antananarivo  
148 Domain and is bound on its east by the Betsileo Shear Zone ( Fig.1b - Collins et al.  
149 2000). It also occurs as an NNW-SSE aligned belt separating the Antananarivo from  
150 the Ikalavony Domain to the west (Figs. 1b and 2). The Itremo Group includes a  
151 series of metasedimentary and metabasic rocks, plus gneisses with late Archaean to  
152 Palaeoproterozoic sources (Cox et al. 1998; 2004a; Fernandez and Schreurs, 2003;  
153 Fitzsimons and Hulscher 2005; Armistead et al. in review). It consists of quartzite,  
154 metadolomite and metapelite. Detrital zircon grains from quartzites present prominent  
155 age peaks at ca. 1850 Ma and ca. 2500 Ma (Cox et al., 1998, 2004b, Fitzsimons and  
156 Hulscher, 2005) with a maximum depositional age of ca. 1700 Ma (Cox et al., 2004a;  
157 Fernandez and Schreurs, 2003). In addition, basic volcanic rocks, interlayered with  
158 metapelites and above the carbonate units (Cox et al., 1998), are intruded by ca. 850–  
159 750 Ma plutonic rocks of the Imorona-Itsindro Suite (BGS-USGS-GLW, 2008; CGS,  
160 2009a, 2009b; Cox et al., 2004b; Fernandez and Schreurs, 2003; Collins et al. 2003c;  
161 Tucker et al., 2007). The Itremo Group was deformed into early recumbent folds, that  
162 either pre-date the Imorona-Itsindro Suite (Collins et al. 2003c) or formed  
163 synchronously with magmatism (Armistead et al., 2020), and refolded into late upright  
164 folds either progressively (Armistead et al., 2020) or much later during the  
165 Cryogenian–Cambrian (Collins et al. 2003c; Tucker et al. 2007).



## 166           **2.2. The Ikalamavony Domain**

167           The NNW-SSE Ikalamavony Domain contains metavolcanosedimentary rocks of  
168 the Ikalamavony Group intruded by, and derived from, the broadly contemporaneous  
169 ca. 1.0 Ga Dabolava suite (Figs. 1b and 2 - CGS, 2009a, 2009b; Cox et al., 2004b;  
170 Tucker et al., 2007, 2011a, 2011b). The Ikalamavony Group is mainly composed of  
171 metapelite, metapsammite and metavolcanic rocks, interpreted as a  
172 volcanosedimentary marginal sequence related to a magmatic arc environment with  
173 a Stenian-Tonian age (ca. 1080–980 Ma; Archibald et al., 2018; Tucker et al., 2011a).  
174 In addition, its detrital zircon age spectra are distinct from the Itremo Group (Tucker  
175 et al., 2011a). The Ikalamavony Group shows a prominent ca. 1.0 Ga source, linking  
176 it to the Dabolava Suite, with only a minor Palaeoproterozoic contribution (Archibald  
177 et al., 2018). Both the Dabolava Suite and the Ikalamavony Group are interpreted as  
178 forming in a subduction-related ca. 1000 Ma island arc setting in the Mozambique  
179 Ocean, outboard of the Archaean to early Palaeoproterozoic shield of Madagascar  
180 (Fig. 1b - Archibald et al., 2018). Then the Ikalamavony domain accreted to the  
181 Malagasy basement before the intrusion of the ca. 850–750 Ma Imorona-Itsindro  
182 Suite (Archibald et al., 2018; Fig. 1b).

183           Another Neoproterozoic metasedimentary unit, the Molo Group, was suggested  
184 by Cox et al. (2004a) based on detrital zircon age populations of three samples  
185 (quartzite, biotite gneiss, hornblende metapsammite). It has a late Meso- to  
186 Neoproterozoic detrital zircon signature, with three major age peaks at ca. 1090–1030  
187 Ma, ca. 840–780 Ma and ca. 690–630 Ma, and with only minor grains that are older  
188 than ca. 1090 Ma. The depositional age of the Molo Group is constrained to between  
189  $613 \pm 9$  Ma (youngest detrital zircon), and  $556 \pm 10$  Ma (average age of the  
190 metamorphic overgrowths; Cox et al. 2001, 2004a).

## 191           **2.4. The SW terranes**

192           The southwestern part of Madagascar there are four distinct tectonic domains  
193 (Boger et al., 2014, 2019): the Anosyen, the Androyen, the Graphite and the Vohibory  
194 (Fig. 1b). The Anosyen Domain is the most extensive and is comprised of two distinct  
195 groups of paragneissic rocks: (a) the Iakora Group—pelitic and calc-silicate gneisses  
196 with terrigenous or chemical sedimentary origin; and (b) the Horombe Group—  
197 extrusive volcanics, or pyroclastic/epiclastic volcanic sedimentary rocks (Boger et al.,  
198 2014). While the siliciclastic sedimentary rocks of the Iakora Group encompass  
199 mostly ca. 2400–1600 Ma aged detrital zircon with a modal age peak at approximately  
200 1850 Ma, the Horombe Group has peraluminous (ca. 1800–700 Ma, Tôlanaro  
201 Formation) and metaluminous (ca. 820–760 Ma, Benato Formation) rocks with ages  
202 similar to the Imorona–Itsindro Suite (Kröner et al., 1999; Tucker et al., 2011a; Collins  
203 et al., 2012; Boger et al., 2014).

204           Published age data from the Androyen Domain are limited. Possible granitic  
205 protolith ages of ca. 2200–1800 Ma (Tucker et al., 2011a, 2014), considerable  
206 Palaeoproterozoic detritus (Collins et al. 2012) and a spread of ages between ca.  
207 620 and ca. 520 Ma are interpreted to reflect two closely spaced (ca. 630–600 Ma  
208 and 580–520 Ma) periods of high-temperature metamorphic zircon growth (Tucker  
209 et al., 2011a; Boger et al., 2015). This domain also includes two groups of stratified  
210 units (Mangoky and Imaloto groups), which are intruded by ca. 930–910 Ma  
211 magmatic rocks from Ankiliabao Suite (GAF-BGR, 2008b).

212           The narrow and elongate Graphite Terrane (Boger et al., 2019) have gneisses  
213 that hosts the Ankiliabo Suite, therefore predating by several hundreds of millions of  
214 years the formation of the intermediate to felsic protoliths of the Vohibory Domain, to  
215 the west (Fig. 1b). In addition, felsic magmas in the Graphite Domain are originated

216 from shallower crustal source rocks (Boger et al., 2019). Strongly positive initial  $\epsilon\text{Nd}$   
217 and relatively low age corrected  $87\text{Sr}/86\text{Sr}(m)$  indicate that the gneisses of the  
218 Graphite Domain, similar to those of the Vohibory Domain, likely formed in an intra-  
219 oceanic environment (Boger et al., 2019).

220 The Vohibory Domain is represented by felsic and mafic orthogneisses, which are  
221 intercalated with paragneisses and marbles (Boger et al. 2019). Mafic orthogneisses  
222 are suggested to represent a blend of mid-ocean-ridge, back-arc and island arc  
223 basalt with inferred extrusion ages between ca. 850–700 Ma (Emmel et al., 2008;  
224 Jöns and Schenk, 2008), while younger felsic gneisses are dated between 670–630  
225 Ma (Boger et al., 2015). In addition, the metasedimentary rocks yield a unimodal  
226 population of detrital zircon with an age range between ca. 900 Ma and ca. 750 Ma  
227 (de Wit et al., 2001; Emmel et al., 2008; Jöns and Schenk, 2008; Collins et al. 2012).  
228 The main metamorphic and deformational phase occurred at ca. 630–600 Ma, with  
229 a minor impacts of a 580–520 Ma orogenic event (Emmel et al., 2008, Jöns and  
230 Schenk, 2008, Collins et al., 2012; Boger et al., 2015).

231

## 232 **2.4. The Imorona-Itsindro magmatic unit**

233 The Antananarivo (including the Itremo Group) and Ikalamavony domains, plus  
234 the Masora Craton, are intruded by Tonian-aged, weakly peraluminous granitic and  
235 gabbroic rocks of the Imorona-Itsindro Suite (Fig. 1b and 2 - Archibald et al., 2016,  
236 2017; Boger et al., 2015; Zhou et al., 2018). These rocks are interpreted as  
237 subduction related (Handke, et al., 1999; Archibald et al. 2016; 2017), with U–Pb  
238 zircon emplacement ages between ca. 850 Ma and ca. 750 Ma, but major magmatic  
239 activity from ca. 800 Ma to 780 Ma (Archibald et al., 2016; Handke et al., 1999;

240 McMillan et al., 2003; Tucker et al., 2011a; Kröner et al. 2000). Its origin is  
241 hypothesized as a result of the convergence between the Archaean nuclei of the  
242 Antongil-Masora cratons (Dharwar Craton – India; Fig 1a) and the Antananarivo  
243 (Malagasy basement) domain, that resulted in the generation of Andean-type  
244 magmatism due to subduction and the closure of the Neoproterozoic Mozambique  
245 Ocean (BGS-USGS-GLW, 2008; Collins, 2006; Collins and Pisarevsky, 2005; Collins  
246 and Windley, 2002; Kröner et al. 2000). The subduction polarity was originally  
247 proposed to be east-dipping, from a trench located to the west and subduction under  
248 the Antananarivo Domain (Handke et al. 1999). A number of authors then  
249 reinterpreted this to indicate west-dipping subduction from a trench located along the  
250 proposed Betsimiaraka Suture separating the Antananarivo Domain from the Antongil  
251 Domain (Fig. 1b - Kröner et al. 2000; Collins and Windley, 2002; Collins et al. 2003a;  
252 Collins and Pisarevsky, 2005; Fitzsimons and Hulscher 2004; Archibald et al. 2016;  
253 2017; Armistead et al. 2018; 2020). In contrast to the subduction origin hypotheses,  
254 Zhou et al. (2015) analysed the chemistry of many fewer intrusions than Archibald et  
255 al. (2016; 2017), but suggested that instead, the suite represents melting of the so-  
256 called Greater Dharwar Craton during mantle plume induced rifting.

257 The southwestern tectonic domains have no record of the ca. 850–750 Ma  
258 Imorona-Itsindro Suite, but age equivalent volcanic or intrusive rocks are present in  
259 the Anosyen Domain (Tucker et al. 2011; Boger et al. 2014). Boger et al. (2014)  
260 interpreted the Imorona-Itsindro magmatic event as related to a subduction zone  
261 located to the west, supporting the original interpretation of Handke et al. (1999), but  
262 contrasting with interpretations of others (Collins, 2006; Collins and Pisarevsky, 2005;  
263 Collins and Windley, 2002; Kröner et al., 2000). Nevertheless, the ca. 550 Ma suture

264 zone is placed between the Androyen and the Anosyten domains (Boger et al., 2015,  
265 2019).

## 266 **2.5. The Ediacaran–Cambrian tectonic overprint**

267 The entire Antananarivo Domain was deformed and metamorphosed up to  
268 granulite facies conditions (e.g. Cenki-Tok et al., 2015) and intruded by Ediacaran-  
269 Cambrian syn- to late-tectonic granitic dykes and plutons of the Ambalavao and  
270 Maevarano plutonic suites (Fig. 1b and 2; Archibald et al., 2019; Paquette and  
271 Nédélec, 1998; Boger et al., 2014; Horton et al., 2016). This major tectonic event was  
272 related to the final Gondwana amalgamation, when the Malagasy shield was the site  
273 of east-directed translation of crystalline nappes, high-grade metamorphism and  
274 widespread magmatism (Tucker et al., 2011b; Collins et al. 2003c). The post-orogenic  
275 plutonic suites intruded between ca. 580 and 520 Ma (Archibald et al., 2019;  
276 Goodenough et al., 2010). Goodenough et al. (2010) interpreted Maevarano Suite as  
277 the final stages of an extensional collapse that followed asthenospheric upwelling.

278 Two events of deformation and high-temperature metamorphism occur in  
279 southwestern Madagascar: one at ca. 620–600 Ma (recorded only in the Androyen  
280 and Vohibory domains) and a second at ca. 580–520 Ma that is widespread in all  
281 domains (Ashwal et al., 1999; de Wit et al., 2001; Jöns and Schenk, 2011). The  
282 second event is accompanied by the emplacement of the Ambalavao Suite (Fig. 1b

283 - Ashwal et al., 1999; de Wit et al., 2001; Emmel et al., 2008; Jöns and Schenk, 2008,  
284 2011; Tucker et al., 2007).

### 285 **3. Method**

#### 286 **3.1. Zircon separation and imaging**

287 Eight samples of approximately 2.5 to 3 kg were collected for petrography and  
288 geochronology. The selected samples were crushed in a jaw crusher, disk mill  
289 grinder, and sieved to zircon fraction between 79–425  $\mu\text{m}$ . After sample crushing,  
290 heavy minerals were separated by manual panning and then using magnet, heavy  
291 liquids technique (methylene iodide – density:  $3.32\text{g}/\text{cm}^3$ ) and Frantz Isodynamic  
292 Magnetic Separator. These steps were performed at the laboratories of University of  
293 Adelaide, Australia. Four samples yielded sufficient zircon grains and were hand-  
294 picked from the heavy mineral fractions. Zircon grains were mounted in a circular  
295 epoxy resin, polished and then imaged in reflected light (RL). Cathodoluminescence  
296 (CL) images were obtained to investigate the internal structure of the zircon grains,  
297 acquired by Philips XL40 Scanning Electron Microscope equipped using a tungsten  
298 filament electron source and a Gatan CL detector attached for high-resolution  
299 imaging at Adelaide Microscopy.

#### 300 **3.2. Zircon U-Pb geochronology**

301 Zircon U-Pb geochronology was performed at Adelaide Microscopy, University  
302 of Adelaide, by Laser Ablation Inductively Coupled Mass Spectrometry (LA-ICP-MS)  
303 using an 7500cs ICPMS unit coupled to a New Wave 213 nm Nd-YAG laser using a  
304 spot size of 30  $\mu\text{m}$  and frequency of 5 Hz. U-Pb-Th isotope fractionation was  
305 corrected using GEMOC GJ-1 zircon ( $^{207}\text{Pb}/^{206}\text{Pb}$  age =  $607.7 \pm 4.3$  Ma,  $^{206}\text{Pb}/^{238}\text{U}$   
306 age =  $600.7 \pm 1.1$  Ma and  $^{207}\text{Pb}/^{235}\text{U}$  age =  $602.0 \pm 1.0$  Ma; Jackson et al., 2004).

307 Data were processed using GLITTER software (Griffin et al., 2008). Concordia  
308 diagrams were produced using IsoplotR (Vermeesch, 2018) and Kernel Density  
309 Estimates (KDE) were produced in R using a bandwidth of 25 Ma. Data within 10%  
310 of concordance are included (Fig. 6). Furthermore,  $^{207}\text{Pb}/^{206}\text{Pb}$  and  $^{206}\text{Pb}/^{238}\text{U}$  ages  
311 were used for zircon grains older and younger than 1.3 Ga, respectively. Probability  
312 density plots from figure were constructed using ISOPLOT 4.15 software in Microsoft  
313 Excel (Ludwig, 2012) with discordance equal or < 10%.

### 314 **3.3. Zircon Lu-Hf analysis**

315         Seventy-nine Lu-Hf isotopes were analysed on the Thermo-Scientific Neptune  
316 Multi-Collector ICP-MS with an attached New Wave 193 Excimer laser ablation  
317 system at the University of Wollongong. A beam diameter of 50  $\mu\text{m}$  was used. Typical  
318 ablation times were ~ 45 seconds using a 5 Hz repetition rate and an intensity of  
319 ~4.40 J/cm<sup>2</sup>. Zircon grains were ablated in a helium atmosphere that was then mixed  
320 with argon upstream of the ablation cell.

321         Plešovice and Mudtank zircon standards were analysed before and during the  
322 analysis of unknowns to assess instrument stability and performance. Twenty  
323 Plešovice standard analyses were made and yield an average of  $0.282471 \pm$   
324  $0.000042$ , which is within uncertainty of the published value of  $0.282482 \pm 0.000013$   
325 by (Sláma et al., 2008). Twenty Mudtank standard analyses were made and yield an  
326 average of  $0.282505 \pm 0.000047$ , which is within uncertainty of the published value  
327 of  $0.282507 \pm 0.000006$  (Woodhead et al., 2004).

328         Zircon data were reduced using lolite and normalised to  $^{179}\text{Hf}/^{177}\text{Hf} = 0.7325$ .  
329 Values for  $^{176}\text{Hf}/^{177}\text{Hf}_{\text{CHUR}(t)}$  were calculated using modern  $^{176}\text{Hf}/^{177}\text{Hf} = 0.282785$   
330 (Bouvier et al., 2008), modern  $^{176}\text{Lu}/^{177}\text{Hf} = 0.0336$  (Bouvier et al., 2008), and  $^{176}\text{Lu}$

331 decay constant of  $1.865 \times 10^{-11} \text{ year}^{-1}$  (Scherer et al., 2001). Values for crustal  
332 model ages ( $T_{\text{DMC}}$ ) were calculated using a  $^{176}\text{Lu}$  decay constant of  
333  $1.865 \times 10^{-11} \text{ year}^{-1}$  (Scherer et al., 2001), modern  $^{176}\text{Hf}/^{177}\text{Hf} = 0.28325$ , modern  
334  $^{176}\text{Lu}/^{177}\text{Hf} = 0.0384$  (Griffin et al., 2002), and a bulk crust value of  $^{176}\text{Lu}/^{177}\text{Hf} = 0.015$   
335 (Griffin et al., 2002). Uncertainties for  $\varepsilon_{\text{Hf}}(t)$  are calculated as the  $^{176}\text{Hf}/^{177}\text{Hf}_{\text{Sample}}$   
336 uncertainty converted to epsilon notation (i.e.  $[(^{176}\text{Hf}/^{177}\text{Hf}_{2\sigma})/0.282785] * 10,000$ ) and  
337 are reported at the  $2\sigma$  level).

## 338 4. Results

### 339 4.1. Geology of the study area

340 The studied area is located 22 km southeast of the village of Ikalamavony (Fig.  
341 2) and includes the contact between the Antananarivo and the Ikalamavony domains  
342 (Fig. 1b and 2). Geological mapping was performed at 1:25,000 scale (Fig. 3) and  
343 the geological units are described below.

#### 344 4.1.1. Metasedimentary units

345 We identified three metasedimentary units, from bottom to top: 1- quartzite  
346 with interleaved (garnet-sillimanite) muscovite-biotite schists; 2- calc-silicate rocks,  
347 and 3- fine-grained plagioclase-biotite paragneiss.

348 The first and structurally lowest sequence comprises aligned NNE-SSW  
349 mountain ranges (Fig. 3 and 4a). Thick layers, up to 5 meters, of pure quartzite  
350 predominate on the bottom (Fig. 4a – samples DA13-039 and DA13-045 – see item  
351 4.1.3 and 4.1.2, respectively). Towards the top, packages of thin layered quartzite  
352 beds, varying from 5 to 10 cm thick (sample DA13-036 – item 4.1.1), are interlayered  
353 with (garnet-sillimanite) muscovite-biotite-schists (Fig. 4b). The thin-layered  
354 quartzites are more micaceous than the thicker beds, with biotite and muscovite (Fig.



355 5a). Accessory minerals such as tremolite occur on layers near the contact with the  
356 upper calc-silicate unit (Fig. 5a).

357 The interleaved (garnet-sillimanite) muscovite-biotite-schists are weathered,  
358 rarely preserving garnet, mostly replaced by oxides (Fig. 4b). The mineral  
359 assemblage indicates sillimanite zone upper amphibolite facies metamorphism  
360 (Fig. 5b and 5c). There is a metamorphic foliation ( $S_n$ ), represented by mica orientation  
361 and stretched quartz grains, parallel to the primary bedding ( $S_0$ ). This foliation locally  
362 transposes crenulation surfaces, which represent an earlier tectonic foliation  $S_{n-1}$   
363 (Fig. 5b and 5c), attesting a polyphase ductile deformation event.

364 The compositional variety of this sequence reflects changes of the  
365 sedimentary protolith, considered here as primary bedding -  $S_0$  (Fig. 4b). Although  
366 there is indication of shearing and transposed foliation, parallel to bedding, the  
367 distribution of facies indicates a fining upward sequence.

368 The second unit is a calc-silicate package structurally above the quartzites  
369 (Fig. 3), composed of dark green rocks (~10 meters thick; Fig. 4c) with intermittent  
370 beds of white marbles, up to 2 meters thick (Fig. 4d), and also impure quartzite, up  
371 to 1 meter thick (Fig. 4e). It is comprised of mainly calcium-rich minerals (Fig. 4c),  
372 such as diopside, amphibole, epidote, and accessory minerals quartz, biotite,  
373 plagioclase and titanite. The unit displays mylonitic foliation and a transposed  
374 crenulation cleavage. At the bottom, a green calc-silicate diopside gneiss is dominant  
375 (Fig. 4c). Towards the top, the rocks show intercalation of coarse-grained white  
376 marble beds, constituted mostly by recrystallized calcite (Fig. 4d). One 2-meter-thick  
377 bed of impure foliated feldspar-bearing quartzite (Fig. 4e).

378 The third supracrustal unit is a fine-grained homogeneous plagioclase-biotite-  
379 paragneiss (Fig. 4f and 4g - sample DA13-030 – item 4.1.4). It comprises layers of up  
380 to 15 meters thick (Fig. 4g), constituted by quartz, plagioclase and biotite (Fig. 5d).  
381 Accessory minerals are white micas, zircon and Fe-oxides. The protolith is interpreted  
382 as a psammitic rock that might have been a fine-grained arkose with plagioclase. The  
383 mineral composition of this unit, plagioclase, quartz and mica, indicates that the  
384 sources were predominantly andesitic. The contact with the calc-silicate unit is  
385 concordant but the beds show high strain and stretching lineation that might indicate  
386 that it is a tectonic contact.

387 The three sedimentary-derived units present a continuous tectonic foliation  
388 dipping W-SW, parallel to compositional layering, with evidence of transposition (Fig.  
389 5b and 5c) related to a down dip stretching lineation. Kinematic indicators suggest a  
390 top to E-NE movement (Fig. 2 and 3).

#### 391 **4.1.2. (Meta) igneous units**

392 Three different (meta) igneous units were recognized in the studied area (Fig.  
393 3): 1- metafelsite tabular bodies, 2- porphyritic orthogneiss, both correlated with the  
394 Imorona-Itsindro Suite; and 3- granite (correlated with Ambalavao Suite - Fig.1b).

395 The metafelsite bodies occur as dykes/sills, usually parallel and subparallel to  
396 the  $S_0/S_n$ , intruding the calc-silicate and the biotite-paragneiss units. They are up to 3  
397 meters thick, and are shown on the geological map as dyke swarms and branches  
398 (Fig. 3 and 4h). They show fine-grained, occasionally porphyritic texture. The  
399 composition is rhyolitic, with quartz, microcline, biotite and muscovite. The dykes have  
400 quartz and K-feldspar as phenocrysts. The metafelsites present a tectonic foliation  
401 and some phenocrysts are also stretched (Fig. 4h). Archibald et al. (2016) dated one

402 sample of this unit (DA13-029), interleaved with the calc-silicate unit, yielding a U-Pb  
403 zircon age of  $828 \pm 14$  Ma that was interpreted as the emplacement age (see location  
404 on Fig. 3).

405 The porphyritic orthogneiss is recognized at the NE portion of the area (Fig. 3)  
406 and exhibits penetrative foliation marked by oriented biotite and stretched quartz. It is  
407 also correlated with the Imorona-Itsindro Suite according to the age obtained by  
408 Archibald et al. (2016) within the studied area ( $758 \pm 10$  Ma – sample DA13-020- also  
409 indicated on Fig. 3). The crosscutting relationships between the orthogneiss and the  
410 quartzitic unit are poorly constrained. Near the contact with the orthogneiss, mafic  
411 dykes with tectonic foliation crosscut the quartzite layers (Fig. 4i).

412 The third igneous unit is represented by a large pluton in the centre of the area  
413 (Fig. 3). These pinkish fine- to medium-grained granodioritic rocks are correlated with  
414 the Ambalavao Suite, and crosscut all other units (Fig. 4j). The rocks are commonly  
415 hololeucocratic and isotropic. Locally, some biotite foliation is recognized. The major  
416 body is dated with U-Pb zircon analysis from two samples, one at  $550 \pm 12$  Ma and  
417 another at  $539 \pm 5.5$  Ma (Archibald et al., 2019). A folded granitic dyke that cross cut  
418 the biotite-paragneiss was also dated at ca. 540 Ma (DA-13-031 – Figs. 3; Archibald,  
419 2019) that is interpreted as the crystallization age (Fig. 4g). The composition and age  
420 of the deformed dyke is similar to the large pluton, therefore, we interpret this as the  
421 same magmatic event. The deformation pattern affected only the thin vein probably  
422 because of thickness and relation with the host rock (Fig. 4g). Although it is folded, it  
423 clearly cross-cuts the metamorphic foliation of the biotite-paragneiss.

424

425

## 426 **4.2. U-Pb detrital zircon data**

427 A total of 511 LA-ICP-MS U-Pb analyses of zircon cores and rims were  
428 randomly performed on 416 detrital zircon grains extracted from four rock samples  
429 (DA-13-045; DA-13-039; DA-13-036; DA-13-030 – Fig. 3). Of all, 307 zircon grains  
430 yielded 294 concordant  $^{207}\text{Pb}/^{206}\text{Pb}$  and/or  $^{206}\text{Pb}/^{238}\text{U}$  ages, with 48 concordant ages  
431 collected from metamorphic rims (Supplementary table 1).

### 432 **4.2.1. Sample DA13-045**

433 This quartzite sample was collected on Route Nationale 7, near Ankaramena  
434 town in the Ambalavao District (Fig. 2), at the lower portion of the quartzite unit (item  
435 2.2.1), near the contact with the Antananarivo Domain basement. It is a massive  
436 quartzite with locally more foliated layers with biotite and tourmaline. It grades  
437 towards the top, westwards, to calc-silicate layers. A quartzite in this outcrop was  
438 also sampled and dated by Tucker et al. (2011a; sample MJY-08-55). They obtained  
439 for 70% of the populations ages modes at 2.55-2.40 Ga, 2.7 Ga and 2.9 Ga. Thirty  
440 per cent of their sample provided age modes at 2.1-2.0 Ga and 1.8 Ga. Fifteen  
441 concordant rims yielded metamorphic ages between 550 and 450 Ma.

442 Our sample shows zircon grains with grain size length from ~120 to 250  $\mu\text{m}$   
443 with aspect ratios of 1:1 and 2:1 (length to width). The external grain morphology is  
444 similar to sample DA13-036, showing sub-rounded grains, with rounded/sub-rounded  
445 xenocrystic cores and homogeneous rims exhibiting a dark CL response (Fig. 7b)  
446 and most of the xenocryst cores show complex internal growth zoning.

447 Eighty analyses were performed on zircon cores and rims, of which 46  
448 analyses yielded ages  $\leq 10\%$  discordant including 36 zircons cores and 10  
449 metamorphic rims obtained from 44 zircon grains (Supplementary table 1).

450  $^{207}\text{Pb}/^{206}\text{Pb}$  ages vary between  $3337 \pm 37$  to  $1784 \pm 26$  Ma and the major  
451 population is within the interval ca. 2160–1820 Ma (15; 41% of the total concordant  
452 analyses) and interval ca. 2690–2400 Ma (13; 36% of the total concordant analyses)  
453 (Fig. 6b). The oldest zircon cores show  $^{207}\text{Pb}/^{206}\text{Pb}$  Paleoarchaeon ages ( $3337 \pm 37$   
454 Ma and  $3222 \pm 21$  Ma; Fig. 7b: #045-059 and #045-010) and 3 grains have  
455 Mesoarchaeon ages ( $3073 \pm 20$  Ma,  $3020 \pm 23$  Ma, and  $2860 \pm 22$  Ma; Fig. 7b: #045-  
456 075, #045-009 and #045-006). The youngest detrital zircon grain has an age of  $1784$   
457  $\pm 26$  Ma.

#### 458 **4.2.2. Sample DA13-039**

459 Sample DA13-039 was collected at the road from the town of Mangidy to  
460 Ikalamavony (Fig. 2). The sample is a coarse-grained quartzite from the lower  
461 sequence within the quartzite unit (described on item 2.2.1). Zircon grain lengths are  
462 between ~120 and 260  $\mu\text{m}$  with aspect ratios of 1:1 and 2:1 (length to width). Sub-  
463 rounded grains, with sub-rounded xenocryst cores and homogeneous rims exhibiting  
464 a black CL response (Fig. 7c), characterize the zircon morphologies for this sample.  
465 Most of the xenocryst cores show complex growth zoning.

466 Ninety-three analyses of zircon cores and rims were performed, of which 71  
467 analysis yielded ages with  $\leq 10\%$  discordance, including 60 zircon cores and 10  
468 metamorphic rims from 65 zircon grains (Supplementary table 1).  $^{207}\text{Pb}/^{206}\text{Pb}$  ages  
469 of concordant analysis vary from  $3099 \pm 52$  to  $2038 \pm 23$  Ma and the main contribution  
470 is ca. 2500 Ma. Three major intervals are observed: ca. 2750–2670 Ma (7 analyses;  
471 ~10% of the total), ca. 2500–2400 Ma (17 analyses; ~24% of the total) and ca. 2300–  
472 2030 Ma (28 analyses; 39% of the total concordant data- Fig. 6). Five concordant  
473 analyses on the oldest zircon grains present Mesoarchaeon  $^{207}\text{Pb}/^{206}\text{Pb}$  ages ranging

474 from  $3099 \pm 52$  Ma to  $2940 \pm 24$ , approximately 7% of all concordant data (Fig. 7c:  
475 #039-074, #039-042 and #039-015). The most significant population of detrital zircon  
476 have Siderian  $^{207}\text{Pb}/^{206}\text{Pb}$  ages between ca. 2500 and 2330 Ma, ~25% of the data  
477 (18 concordant ages; Fig. 6). The youngest detrital zircon core yielded an age of  
478  $2038 \pm 23$  Ma (Fig. 7c: #039-007).

#### 479 **4.2.3. Sample DA13-036**

480 Sample DA13-036 was collected at the road between the town of Mangidy and  
481 Ikalamavony, near the junction to Solila (Fig. 2). The sample is a quartzite from the  
482 structurally lowest sequence containing tremolite (described on item 2.2.1). The  
483 detrital zircon grains have grain size length from ~ 110 to 230  $\mu\text{m}$  with aspect ratios  
484 of 1:1 and 2:1 (length to width). Sub-rounded grains, with rounded/sub-rounded  
485 xenocryst cores and blackish homogeneous rims (Fig. 7a), characterize the external  
486 zircon morphology. Xenocryst cores show complex internal growth zoning.

487 One-hundred zircon cores and rims were analysed, of which 80 analyses  
488 yielded ages that are  $\leq 10\%$  discordant, including 57 zircon cores and 23  
489 metamorphic rims from 65 zircon grains (Supplementary table 1).  $^{207}\text{Pb}/^{206}\text{Pb}$  ages  
490 vary from  $3358 \pm 36$  to  $1814 \pm 40$  Ma and the most abundant ages are between ca.  
491 2700 and 1900 Ma. The probability density plot presents two major age intervals at  
492 ca. 2250–1810 Ma (25 analyses, ~31% of the total concordant ages) and ca. 2680–  
493 2390 Ma (27 analyses, ~34% of the total) (Fig. 6). This latter group represents the  
494 most significant number of detrital zircon grain ages, with a peak of  $^{207}\text{Pb}/^{206}\text{Pb}$  ages  
495 between ca. 2590–2390 Ma consisting of 26% of the total data (21 concordant ages).

496 There is one zircon core with a Palaeoarchaeon  $^{207}\text{Pb}/^{206}\text{Pb}$  age ( $3358 \pm 36$   
497 Ma; Fig. 7a: #036-039) and another with Mesoarchaeon age ( $2914 \pm 21$  Ma; Fig. 7a:

498 #036-094). The youngest detrital zircon core yielded an age of  $1814 \pm 40$  Ma (Fig.  
499 7a: #036-010). Only one detrital zircon grain has a Th/U ratio lower than 0.1 (0.03;  
500 Fig. 7a: #036-021), within a homogenous CL-domain presumably a metamorphic  
501 grain of 2.5 Ga.

#### 502 **4.2.4. Sample DA13-030**

503 Sample DA13-030 was collected near Solila junction, south of the road from  
504 Mangidy to Ikalamavony (Fig. 2 and 3). The sample is a fine-grained homogeneous  
505 plagioclase-biotite paragneiss (described on item 2.2.1). The detrital zircon  
506 population shows grain size lengths varying from ~90 to 340  $\mu\text{m}$  with aspect ratios of  
507 1:1 and 2:1 (length to width). In terms of morphology, the detrital zircon grains are  
508 very distinct from the previous three samples. In general, external zircon morphology  
509 shows mostly poorly rounded grains and rarely rounded grains (Fig. 7d). Sometimes  
510 zircon grains have sub-rounded to rounded xenocryst cores showing complex growth  
511 zoning. However, the predominant internal structure is the typical igneous oscillatory  
512 zoning (Fig. 7d).

513 For this sample, 238 analyses on zircon cores and rims were performed, of  
514 which 147 analyses yielded ages that are  $\leq 10\%$  discordant, including 143 zircon  
515 cores and some igneous rims, plus four metamorphic dark rims. All data was  
516 obtained from 133 zircon grains.  $^{207}\text{Pb}/^{206}\text{Pb}$  ages of concordant analyses vary from  
517  $2708 \pm 40$  Ma to  $709 \pm 11$  Ma (Supplementary table 1). The most significant  
518 population presents Tonian–Cryogenian ages varying from ca. 860 to 710 Ma (Fig.  
519 6d; 93 analyses; 65% of all concordant data). A minor contribution is represented by  
520 the interval ca. 2.7 to 1.8 Ga (Fig. 6d), with a Siderian peak of ca. 2.5–2.4 Ga (16  
521 analyses; ~11% of all concordant data). The oldest detrital zircon is Neoproterozoic in

522 age ( $2708 \pm 40$  Ma; Fig. 7d: #030-163), that together with other 11 Neoarchaean  
523 zircon grains represent ~8% of the total concordant analyses. Some of these zircon  
524 grains have Th/U ratios lower than 0.1 (3 analyses; ~2% of all data) (Fig. 7d: #030-  
525 074, #030-219 and #030-220). These metamorphic detrital grains have ages of  $1826$   
526  $\pm 39$  Ma,  $809 \pm 11$  Ma, and  $753 \pm 10$  Ma respectively.

### 527 **4.3. U–Pb metamorphic ages**

528 Metamorphic rims were analysed in the detrital zircon population from all four  
529 samples, and 46 ages were obtained (Supplementary table 1). These concordant  
530 ages vary from  $616 \pm 8$  Ma (Fig. 8c: #045-070 – oldest rim) to  $504 \pm 6$  Ma (Fig. 8c:  
531 #036-009 – youngest rim). There is a significant distinction between the three  
532 samples from the quartzite unit (DA13-036, DA13-045 and DA13-039) and the  
533 sample from the paragneiss unit (DA13-030). The latter shows very thin dark  
534 metamorphic rims that surround the mostly prismatic detrital grains. These thin rims  
535 were difficult to date with the LA-ICP-MS technique (Fig. 7d and 8c). They have Th/U  
536 ratios between 0.03 and 0.08. Only three spots were analysed giving ages of:  $614 \pm$   
537  $8$  Ma,  $598 \pm 8$  Ma and  $581 \pm 8$  Ma (Fig. 8c).

538 The three samples from the quartzite unit show thick, dark metamorphic rims  
539 that truncate the internal morphology of the rounded to sub-rounded detrital zircon  
540 cores (Fig. 7a, 7b, 7c and 8c). We obtained 43 ages from the metamorphic rims of  
541 these samples constraining an interval between ca. 620 to 500 Ma, with weighted-  
542 average age of  $550 \pm 8$  Ma (Fig. 8a and 8b). The Th/U ratios for these metamorphic  
543 rims are 0.18-0.09, for sample DA13-036; 0.01 and 0.04 for sample DA13-045, and  
544 0.01–0.02 for sample DA13-039. Sample DA13-045 has one rim analysis with a Th/U  
545 ratio of 0.21 (Fig. 7b: 045-047).



#### 546 4.4. Lu–Hf data

547 We performed 79 Lu–Hf in zircon analyses on the same four samples  
548 analysed for U–Pb (Supplementary table 2, Fig. 9). Most of the analyses were done  
549 on the detrital zircon grains and two analyses on metamorphic rims (Fig. 7a: #036-  
550 003 and #036-046). The spots were located on the same growth domain as the U-  
551 Pb analysis spot, characterized by the same internal growth pattern (Fig. 7).

552 The three quartzite samples have a similar Hf signature from their detrital  
553 populations (Fig. 9). The Palaeo- to Mesoarchaeon populations (ca. 3.33–2.86 Ga),  
554 show juvenile signatures with  $\varepsilon_{\text{Hf}}(t)$  ranging from +6.8 to -2.1 and  $T_{\text{DM}}$  Hf model ages  
555 between 3.5 and 3.0 Ga. The Mid to Late Neoarchaeon grains (ca. 2.75–2.60 Ga)  
556 show  $\varepsilon_{\text{Hf}}(t)$  values ranging from +7.4 to -7.0 and  $T_{\text{DM}}$  Hf model ages between ca. 3.6  
557 and 2.7 Ga, suggesting both a juvenile and crustal contribution for the detrital zircons.  
558 In the transition between Archaean and Palaeoproterozoic through to the Siderian  
559 period (ca. 2.53 Ga – 2.34 Ga) the detrital population has  $\varepsilon_{\text{Hf}}(t)$  values ranging from  
560 +1.4 to -17.8 and  $T_{\text{DM}}$  Hf model ages between 2.9 and 3.9 Ga. This large variation  
561 from slightly juvenile to evolved Hf isotopic signatures are common in all three  
562 samples. The Rhyacian (2.3–2.05 Ga) to Orosirian (2.05–1.8 Ga) sources exhibit  
563 smaller variation, with U–Pb ages between ca. 2.29 to 1.78 Ga and  $\varepsilon_{\text{Hf}}(t)$  ranging from  
564 +2.0 to -12.9 with  $T_{\text{DM}}$  Hf model ages between 3.6 and 2.6 Ga. However, the Hf  
565 isotopic signature is more evolved, differing from the older Archaean grains.

566 Sample DA13-030 is the only sample that shows a Neoproterozoic detrital  
567 population. The grains analysed for Lu–Hf have U–Pb ages between ca. 1.01 Ga and  
568 0.75 Ga. There is a strong variation on the nature of the sources with  $\varepsilon_{\text{Hf}}(t)$  ranging  
569 from -0.5 to -29.2 and  $T_{\text{DM}}$  Hf model ages between ca. 3.4 and 1.8 Ga. Two groups  
570 can be identified (Fig. 9). The older group with U-Pb ages from 1.01 Ga to 0.89 Ga

571 is more juvenile. The second and youngest group of analysis, with U–Pb ages from  
572 0.82 Ga to 0.75 Ga is much more evolved with high negative  $\varepsilon_{\text{Hf}}(t)$  values. This  
573 sample also contains some older detrital grains. The Siderian sources (2.53–2.38  
574 Ga) have  $\varepsilon_{\text{Hf}}(t)$  values varying from +7.0 and -1.7 with  $T_{\text{DM}}$  Hf model ages between  
575 3.1 Ga and 2.5 Ga, suggesting a more juvenile nature, similar to the quartzite zircons.  
576 The Mid to Late Palaeoproterozoic (2.05–1.83 Ga) detrital zircons present more  
577 crustal contribution with  $\varepsilon_{\text{Hf}}(t)$  varying from -7.2 to -13.4 and  $T_{\text{DM}}$  Hf model ages  
578 between 2.9 Ga and 3.4 Ga, also showing similarities with the quartzite data.

579

## 580 **5. Discussion**

581 The detrital zircon data from the supracrustal rocks in this study define two  
582 different age groups: one group with predominant Palaeoproterozoic peaks and no  
583 Neoproterozoic contribution (DA13-036, DA13-039 and DA13-045); and one sample  
584 with a major early Neoproterozoic age population (Tonian; DA13-030).

### 585 **5.1. Stratigraphic correlation**

586 The three samples of the first group belong to the same stratigraphic quartzite  
587 unit that overlies the western limit of the Antananarivo domain (Figs. 1b and 2). Two  
588 samples (DA13-039 and DA13-045) were collected at the base, near the contact with  
589 the Antananarivo basement, and sample DA13-036 was obtained at the upper part  
590 of the sequence, where the quartzite is interlayered with (garnet-sillimanite)  
591 muscovite-biotite schists (Figs. 3 and 4b). This variation in rock type and, therefore,  
592 the sedimentary protolith, indicates a fining upward sequence. The U–Pb detrital  
593 zircon data show populations of ca. 2.5 Ga, ca. 2.1 Ga, with a minor contribution of  
594 ca. 3.3–2.9 Ga aged zircon and an absence of Neoproterozoic grains. This  
595 provenance pattern is similar to the (meta)sedimentary rocks from the Itremo Group  
596 (Fig. 10; Cox et al., 1998, 2004b; De Waele et al., 2011; Fitzsimons and Hulscher,  
597 2005; Tucker et al., 2011a; Armistead et al. in review). Therefore, it indicates that the  
598 NNW-SSE-oriented belt of the Itremo Group may continue southwards following the  
599 main thrust that separates it from the crystalline rocks of the Antananarivo domain  
600 (Fig. 1b and 2).

601 Tucker et al. (2011a) dated a sample of the quartzite sequence from  
602 Ankaramena (Fig. 2), at the same outcrop where we sampled DA13-045 and  
603 obtained similar data. They also suggested that these quartzites may correlate with  
604 the Itremo Group and are separated from other feldspathic metasedimentary rocks

605 of the Ikalamavony Domain by a significant unconformity. Alternatively, we could  
606 posit that these rocks are tectonic slices of the Itremo Group intercalated with the  
607 younger ca. 1.0 Ga paragneisses from the Ikalamavony Group during the late  
608 Neoproterozoic convergent tectonics. Other possibility is that these quartz-rich clastic  
609 protoliths are related to the Ikalamavony Group, and deposited in the Tonian, but  
610 derived exclusively from Archaean and Palaeoproterozoic source rocks. We note that  
611 these different interpretations have significant implications for whether the  
612 Ikalamavony Domain originated as an exotic volcanic island arc (Tucker et al. 2014;  
613 Archibald et al. 2018) or formed on the margin of the Antananarivo Domain.

614 In the studied area, a two-metre thick quartzite layer within a calc-silicate unit,  
615 above the quartzite unit, showed a detrital zircon pattern similar to the quartzite  
616 samples analysed here (Armistead et al., in review - Fig. 4e; sample MAD17-11-4A).  
617 This calc-silicate unit, composed of diopside gneiss interlayered with coarse-grained  
618 white marble layers, is here interpreted also as part of the Itremo Group (Fig. 3, 4c  
619 and 4d).

620 The depositional age window for the quartzite samples from the Itremo Group  
621 is wide, in between the youngest detrital zircon that is  $1784 \pm 26$  Ma (#045-043;  
622 Supplementary table 1), the age of the metamorphic rims ( $550 \pm 8$  Ma; Fig. 8), and  
623 the age of the crosscutting Ambalavao granite, dated in the area by Archibald et al.  
624 (2019), at  $549 \pm 9$  Ma and  $544 \pm 7$  Ma (samples DA13-037 and DA13-038; Fig. 3). It  
625 is likely that this window can be narrowed by considering that these quartzites are  
626 crosscut by the ca. 850–750 Ma Imorona-Itsindro Suite (Archibald et al., 2016, 2017)  
627 elsewhere in the Itremo Group outcrop (Collins et al. 2003c). This large time gap  
628 allows various interpretations for the depositional history of the Itremo basin (Tucker  
629 et al., 2011a, Boger et al., 2014; Armistead et al., in review).

630 Our second group is represented by the plagioclase-biotite paragneiss (Figs.  
631 3 and 4f - DA13-030), that shows a major detrital zircon population of Tonian-age  
632 (ca. 860–710 Ma), with minor peaks of Neoproterozoic-Palaeoproterozoic ages and a  
633 single Mesoproterozoic grain (ca. 1500 Ma). This pattern is in contrast to the samples  
634 from the Itremo Group, with a major Palaeoproterozoic source (Fig. 6).

635 Based on the younger detrital zircon age and the few metamorphic rims dated  
636 in this sample, the deposition of this unit is constrained to the Cryogenian–early  
637 Ediacaran (ca. 710–610 Ma; Fig. 6 and 8). The plagioclase-biotite paragneiss is also  
638 crosscut by a folded granitic dyke dated at ca. 540 Ma (DA13-031; D.B. Archibald  
639 unpublished data; Figs. 3 and 4g). This age coincides with the metamorphic rims of  
640 the dated samples (Fig. 8).

641 Archibald et al. (2016) obtained a U–Pb zircon crystallization age of  $828 \pm 14$   
642 Ma for metafelsite bodies dykes/sills that intruded parallel and subparallel to the main  
643 foliation within the calc-silicate unit, included here in the Itremo Group (DA13-029 -  
644 Fig. 3 and 4h). These metafelsites are parallel to the plagioclase-biotite paragneiss  
645 and were not observed crosscutting them. To the NE of the area, Archibald et al.  
646 (2016) dated a porphyritic orthogneiss at  $758 \pm 10$  Ma (sample DA13-020; Fig. 3)  
647 and correlated it with the Imorona-Itsindro Suite. This age overlaps with the youngest  
648 detrital zircon population that we dated in the paragneiss (Fig. 6).

649 One striking point is the consistent morphology of the detrital zircon grains  
650 from the plagioclase-biotite gneiss (DA13-030). They are predominantly subhedral  
651 with weakly rounded terminations, well-developed oscillatory zoning and with Th/U  
652 ratios higher than 0.1. The main age range is ca. 860–710 Ma (Fig. 11), same as the  
653 Imorona-Itsindro Suite. Sample DA-13-030 has  $\varepsilon_{\text{Hf}}(t)$  values ranging from -15.1 to -  
654 29.2 and  $T_{\text{DM}} \text{ Hf}$  model ages between ca. 2.6 and 3.4 Ga (Fig. 9). The  $\varepsilon_{\text{Hf}}(t)$  for the

655 Imorona-Itsindro suite rocks (ca. 850–750 Ma) are between -4 to +14.0 in the  
656 Ikalamavony Domain and -7 to -37.3 in the Antananarivo Domain (Archibald et al.,  
657 2016). We therefore suggest that these detrital zircons were likely sourced from the  
658 Imorona-Itsindro Suite plutonic rocks or derived from coeval volcanic rocks erupted  
659 at the same time magmatic event.

660 In addition, some of the igneous zircons from the Tonian-aged detrital zircon  
661 population have cores with very distinct growth patterns and ages between ca. 2.70  
662 to 1.82 Ga, with one analysis of ca. 1.54 Ga (Fig. 7d). Tonian-aged domains with  
663 magmatic oscillatory zoning mantling these zircon cores support as well the  
664 derivation from the Imorona-Itsindro magmatic event (Fig. 7d). Consequently, the  
665 Neoproterozoic to the Palaeoproterozoic cores could be interpreted as xenocrysts  
666 within ca. 860–710 Ma igneous zircons. This reinforces the continental nature of the  
667 Imorona-Itsindro Suite magmatism, which is predominantly non-juvenile (Archibald  
668 et al., 2016; 2017).

669 Sample DA-13-030 also has a minor population of ca. 1.00–0.91 Ga igneous  
670 detrital zircons, with  $\varepsilon_{\text{Hf}}(t)$  varying from -0.5 to -5.1 and  $T_{\text{DM}}$  Hf model ages between  
671 2.1 and 1.8 Ga, representing a slightly evolved source (Fig. 9). This group overlaps  
672 with the age and Hf isotope signature of the Dabolava magmatic suite (ca. 1.08–0.98  
673 Ga; Fig. 11), which is considered to be the main source for the Ikalamavony Group  
674 (Archibald et al., 2018; Tucker et al., 2007). The Dabolava Suite has  $\varepsilon_{\text{Hf}}(t)$  varying  
675 from +15 to +5 (Archibald et al., 2018, Tucker et al., 2011a). Therefore, the zircon  
676 source for the paragneiss are slightly more isotopically evolved than the igneous  
677 rocks of the Dabolava Suite. Therefore, this paragneiss cannot be included in the  
678 Ikalamavony Group, to the west (Ikalamavony domain - Fig. 1b and 2), that shows a

679 unimodal ca. 1.0 Ga contribution and is cross cut by a rhyolite layer dated at ca. 1015  
680 Ma (CGS, 2009a).

681         According to published geological maps from Central Madagascar (e.g. Roig  
682 et al., 2012), this sample would be part of the Ikalamavony Group (Fig. 1b and 2).  
683 However, our data don't fully support this, because the major population of detrital  
684 zircon is ca. 800 Ma, whereas the Ikalamavony Group is dominated by ca. 1.0 Ga  
685 detritus. Therefore, the mapped 'Ikalamavony Group' that covers much of the  
686 Ikalamavony Domain may well contain more than one supracrustal unit of different  
687 age and depositional environment (as originally proposed in Cox et al. 2004a, Tucker  
688 et al., 2011, Boger et al., 2014). The Ediacaran-Cambrian tectonic event then  
689 intercalated these distinct lithostratigraphic groups, hindering the geological  
690 interpretation without more detailed mapping and geochronological controls.

691         Consequently, data from sample DA13-030 indicate that there is an Early  
692 Cryogenian supracrustal unit, not previously described in this region, interpreted here  
693 as volcanoclastic in origin, coeval to the major magmatic event of the Imorona-Itsindro  
694 Suite at ca. 850–750 Ma. The detrital age spectra is similar to the Manampotsy Group  
695 (to the east), but with an important discrepancy (Fig. 1b and 10). In the Manampotsy  
696 Group, the major detrital zircon population is Archaean-Palaeoproterozoic in age  
697 (BGS-USGS-GLW, 2008), which might be related to the basin being located in  
698 between Antongil/Masora cratons and Antananarivo domain (Fig. 1b).

699         Another supracrustal unit correlative would be the Late Neoproterozoic Molo  
700 Group that shows few Archaean and Palaeoproterozoic age modes, together with a  
701 more abundant Neoproterozoic detrital zircon population (Fig. 10; Cox et al., 2004a).  
702 The dated Molo sample was collected close to Ankaramena (Fig. 2), but differs from

703 our unit since it contains younger detrital zircons (ca. 613 Ma) and age populations  
704 of ca. 1000 Ma, ca. 800 Ma and ca. 650 Ma (Fig. 10).

705 Within the southwestern Malagasy tectonic domains, two supracrustal units  
706 have similar geological characteristics and geochronological data to the sample DA-  
707 13-030. The Benato formation from the Anosyen Domain (Fig. 1b) is composed of  
708 quartz-feldspathic paragneisses with volcanic arc geochemical signature and  
709 volcanic zircon ages of ca. 796–626 Ma, interpreted to represent the  
710 extrusion/deposition of the Benato Formation (Boger et al., 2014). It differs from our  
711 sample, due to the lack of older zircons (e.g. 1.0 Ga, 2.2. Ga). The other unit is the  
712 Vohibory series, in the Vohibory Domain (Fig. 1b), that consists of metasedimentary  
713 rocks with marbles and juvenile amphibolite (Collins et al., 2012). Detrital zircon ages  
714 here range between ca. 900–750 Ma. This series is interpreted as deposited during  
715 the Cryogenian with Late Tonian to Cryogenian sources in an intra oceanic-arc  
716 setting that formed between the Antananarivo Domain and the Tanzania Craton  
717 (Collins et al., 2012; Fig. 1a). The difference from our sample is the lack of older  
718 zircon sources and all detritus in the Vohibory metasedimentary rocks can be  
719 correlated with local sources in the Vohibory Domain.

## 720 **5.2. Potential Pre-Neoproterozoic sources**

721 The Pre-Neoproterozoic zircons from all four samples are here correlated with  
722 the major Precambrian crustal blocks of central-east Gondwana (Fig. 1a and 10)  
723 including the Tanzania Craton (Africa), Dharwar Craton (India), Antongil-Masora  
724 blocks (Madagascar), and the Antananarivo Domain (Madagascar).

725 There are three Palaeoarchaeoan detrital zircons (samples DA13-036 and  
726 DA13-045) with U–Pb ages between ca. 3.35 and 3.22 Ga with  $\epsilon_{\text{Hf}}(t)$  varying from



727 +6.8 to +1.9 and  $T_{DM}$  Hf model ages between 3.5 Ga and 3.3 Ga. Similar juvenile  
728 detrital zircons are found in metasedimentary rocks throughout the Dharwar Craton  
729 with  $\varepsilon_{Hf}(t)$  varying from +8 to -4 (Fig. 1a - Armistead et al., 2018; Lancaster et al.,  
730 2015; Maibam et al., 2016; Sarma et al., 2012). However, isotopically juvenile  
731 igneous rocks of this age in the Dharwar Craton are not recognized (Collins et al.,  
732 2015; Glorie et al., 2014; Mohan et al., 2014; Praveen et al., 2014; Yang et al., 2015).  
733 Similar rare Palaeoarchaeon grains are found in the Southern Irumide Belt of Zambia  
734 (along the southern margin of the Congo-Tanzania-Bangweulu Block; Alessio et al.,  
735 2019). Supracrustal rocks with similar detrital zircon ages and Hf isotopic values are  
736 found in the Tanzania craton (Thomas et al. 2016).

737 The Mesoarchaeon population (ca. 3.2–2.8 Ga), from samples DA13-036,  
738 DA13-039 and DA13-045, has  $\varepsilon_{Hf}(t)$  values varying between +5.3 to -2.1 and  $T_{DM}$  Hf  
739 model ages between 3.5 Ga and 3.1 Ga. The Antongil and Masora domains, in  
740 eastern Madagascar (Fig. 1b), contain ca. 3200–3000 Ma igneous rocks that are  
741 interpreted to have been part of the Dharwar Craton at the time (Armistead et al.,  
742 2018; Schofield et al., 2010; Tucker et al., 1999, 2014). These transitional juvenile to  
743 crustal sources occur throughout the Dharwar Craton with  $\varepsilon_{Hf}(t)$  varying from ~ +7 to  
744 -12 (Armistead et al., 2018; Collins et al., 2015; Glorie et al., 2014; Lancaster et al.,  
745 2015; Maibam et al., 2016; Mohan et al., 2014). Alternatively, these zircon grains  
746 could have been derived from the Tanzania Craton, which hosts a range of late  
747 Mesoarchaeon aged igneous zircons (ca. 2820–2610 Ma) with  $\varepsilon_{Hf}(t)$  varying from ~  
748 +4.0 to -5.0 (Thomas et al., 2016).

749 The Mid-Neoarchaeon to Mid-Siderian population (ca. 2.7 to 2.3 Ga) is more  
750 abundant in samples DA13-036, DA13-039 and DA13-045 with  $\varepsilon_{Hf}(t)$  varying from  
751 +7.4 to -17.8 (but predominantly between +2 and -8), and  $T_{DM}$  Hf model ages

752 between 3.9 Ga and 2.5 Ga (Figs. 6 and 9). In addition, sample DA13-030 also  
753 contains a minor population in this interval between 2.70 Ga and 2.34 Ga with  $\varepsilon_{\text{Hf}}(t)$   
754 varying from +7.0 to -1.7 and  $T_{\text{DM}}$  Hf model ages between 3.1 Ga and 2.5 Ga (Fig. 6  
755 and 9). The best source candidate for these zircon grains is the Betsiboka Suite of  
756 the Antananarivo Domain (Figs. 1b and 10). Similar ages and Hf values occur in the  
757 Dharwar Craton, which show  $\varepsilon_{\text{Hf}}(t)$  values varying from +8 to -12 (Glorie et al., 2014;  
758 Praveen et al., 2014; Yang et al., 2015). In contrast, there is no record in the Tanzania  
759 craton of igneous rocks with ages between 2.6–2.3 Ga (Fig. 10; Thomas et al., 2016).

760 The Mid-Rhyacian to Mid-Orosirian population (ca. 2.2 to 1.8 Ga) is also  
761 significant (Figs. 6 and 9). Samples DA13-036, DA13-039 and DA13-045 have U–Pb  
762 ages between 2.29 Ga and 1.78 Ga with  $\varepsilon_{\text{Hf}}(t)$  varying from +2.0 to -12.9 and  $T_{\text{DM}}$  Hf  
763 model ages between 3.3 Ga and 2.6 Ga. Sample DA13-030 has detrital zircons with  
764 U–Pb ages between 2.26 Ga and 1.82 Ga with  $\varepsilon_{\text{Hf}}(t)$  varying from -7.2 to -13.4 and  
765  $T_{\text{DM}}$  Hf model ages between 3.4 Ga and 2.9 Ga. The Hf isotopic data show a trend  
766 from more juvenile, older sources to more evolved, younger zircon sources (Fig. 9).  
767 In addition, sample DA13-030 has two age groups. One group has ca. 2.0 Ga U–Pb  
768 ages with lower  $\varepsilon_{\text{Hf}}(t)$  values (-11.6 and -13.4) and  $T_{\text{DM}}$  Hf model ages between 3.4  
769 Ga and 3.3 Ga. Another group has U–Pb ages of ca. 1.8 Ga with slightly higher  $\varepsilon_{\text{Hf}}(t)$   
770 values (-7.2 and -7.3) and  $T_{\text{DM}}$  Hf model ages between 3.0 Ga and 2.9 Ga. This  
771 indicates two distinct crustal sources. Sample DA13-039 has only U–Pb detrital  
772 zircon grains dated between ca. 2.29–2.03 Ga with negative  $\varepsilon_{\text{Hf}}(t)$  values and  $T_{\text{DM}}$  Hf  
773 model ages between ca. 3.6 Ga and 2.8 Ga. A possible source for these zircons is  
774 the igneous rocks from the Usagaran Belt that marks the eastern Tanzania Craton  
775 with ca. 2.0–1.8 Ga ages and  $\varepsilon_{\text{Hf}}(t)$  values between 0 and -6 (Figs. 1b and 10; Reddy  
776 et al. 2003; Thomas et al., 2016).

777 For the Mesoproterozoic Era, a single grain in sample DA13-030 has U–Pb age  
778 of 1.54 Ga but no Hf data (#030-221 – Supplementary table 1). The Dharwar Craton  
779 has no record of magmatism or detrital zircon grains of this age. Thomas et al. (2016)  
780 describe magmatic rocks of ca. 1.5 Ga in the Tanzania Craton.

781 We can here conclude that the sources for the three quartzite samples,  
782 correlated with the Itremo Group, could be derived either from the eastern cratons  
783 (Dharwar, Antongil, Masora) and/or the western craton (Tanzania; Fig. 1a). The  
784 Palaeoproterozoic and Mesoproterozoic detrital zircon populations could have come from  
785 both the Dharwar and the Congo-Tanzania-Bangweulu cratonic sources (Fig. 1a).  
786 The Neoproterozoic sources (ca. 2.8 to 2.5 Ga), are present today in India and eastern  
787 Madagascar blocks, including the Antananarivo Domain (e.g. Betsiboka Suite - BGS-  
788 USGS-GLW, 2008; Kabete et al., 2006; Kroner et al., 2000; Tucker et al., 1999,  
789 2007). The younger Palaeoproterozoic sources (ca. 2.2 to 1.8 Ga) are abundant only  
790 in the Tanzania Craton (Thomas et al., 2016). Cox et al. (1998, 2004a, 2004b) and  
791 Fitzsimons and Hulscher (2005) proposed correlation between the Antananarivo  
792 Domain and the Tanzania Craton. Collins and Pisarevsky (2005) described a  
793 Neoproterozoic to early-Palaeoproterozoic igneous province comprising present-day  
794 Saudi Arabia, Madagascar and southern India and named this continental block  
795 Azania, composed primarily of ca. 2.45–1.90 Ga rocks (Collins et al., 2001; Collins  
796 and Pisarevsky, 2005; Kroner et al., 1999, 2000; Küster et al., 1990; Lenoir et al.,  
797 1994; Paquette and Nédélec, 1998; Teklay et al., 1998; Whitehouse et al., 2001).  
798 Our data are inconclusive but indicate that the sources for the Itremo-correlated  
799 quartzite do not easily fit with exclusively “Dharwar” or “Tanzanian” sources. However,  
800 the abundant late Palaeoproterozoic detritus that define the maximum depositional  
801 age, and may be close to the age of deposition (Cox et al., 1998), are most strongly

802 correlated with similar sources for the Irumide and Southern Irumide belts of the  
803 Congo-Tanzania-Bangweulu Block (Alessio et al. 2019; Armistead et al. in review).  
804 It seems apparent that by ca. 1.7 Ga, a stable basin was developed that was  
805 predominantly sourcing African Palaeoproterozoic sources, with perhaps some  
806 contribution from recycled, older detritus.

807         The maximum depositional age for our three quartzite Itremo Group samples  
808 is marked by the youngest detrital zircon grain of  $1784 \pm 26$  Ma. This is coherent with  
809 the depositional age proposed for the Maha Group, a package of Palaeoproterozoic  
810 metasedimentary rocks that overlies (perhaps tectonically) the Archaean rocks of the  
811 Masora Domain (Fig. 1b; BGS-USGS-GLW, 2008; Tucker, et al., 2011b). The Maha  
812 Group has ca. 2770 Ma to ca. 1800 Ma detrital zircon populations and a maximum  
813 depositional age of  $1797 \pm 18$  Ma (Fig. 10; De Waele et al., 2011). We also follow  
814 Archibald et al. (2015) in correlating the Ambatolampy Group as a part of this  
815 supracrustal metasedimentary package including the Itremo and Maha groups (max.  
816 dep age 1.8 Ga; Archibald et al., 2015).

817         The similar pattern of detrital zircons sources, plus the maximum depositional age  
818 of ca. 1.7 Ga, for these three groups—Itremo (Antananarivo Domain), Ambatolampy  
819 (Antananarivo Domain) and Maha (Masora Craton)—suggest that they could be  
820 related to the same sedimentary basin (Figs. 1b and 10). In addition, the basin can  
821 be extended to include the Iakora Group (Anosyten Domain) in southern Madagascar  
822 (Boger et al., 2014) and the Sambirano–Sahantaha Group from the southern  
823 Bemarivo Domain (De Waele et al., 2011; Boger et al., 2014; Armistead et al., 2019),  
824 which is thrust onto the Antongil Craton, to the north (Fig. 1b; Schofield et al., 2010;  
825 Thomas et al., 2009; Armistead et al., 2019). These metasedimentary packages have  
826 similar late Palaeoproterozoic maximum depositional ages (Fig. 1b; Collins et al.,

827 2012; Boger et al., 2014; De Waele et al., 2011). Taken together, they appear to  
828 represent an originally contiguous Palaeoproterozoic to early Mesoproterozoic  
829 sedimentary basin across and/or on the margins of Madagascar.

830 The minimum depositional age of this basin or basins is ca. 0.85 Ga as  
831 constrained by the emplacement of the ca. 850–750 Ma Imorona-Itsindro magmatic  
832 suite. The Dabolava Suite (ca. 1080–980 Ma) does not crosscut any of these  
833 formations. This is part of the logic to suggest that the Ikalamavony Domain and,  
834 thus, the Dabolava Suite formed exotic to the rest of Madagascar (Tucker et al. 2014;  
835 Archibald et al., 2016, 2018). Furthermore, the predominantly quartzite nature of the  
836 arenites within the Itremo Group and equivalents, differ lithologically from the Tonian-  
837 aged sedimentary rocks that formed coeval with the Dabolava Suite (Ikalamavony  
838 Group). The latter usually contain appreciable feldspathic and lithic grains and are  
839 interbedded with volcanic rocks that are distinct from the Itremo, Ambatolampy and  
840 Maha groups. The proposed sedimentary environment for the Itremo Group is a  
841 stable shelf with quartz arenites, pelites and carbonate rocks—possibly a passive  
842 margin succession. This suggests a tectonically quiescent period from ca. 1700 to  
843 ca. 850 Ma in the Antananarivo Domain (Tucker et al., 2014).

844 Alternatively, it could be argued that the quartzites mapped by us as the Itremo  
845 Group (Fig. 2) are part of the same sequence as the structurally overlying plagioclase-  
846 biotite paragneiss (mapped as the Ikalamavony Group in Fig. 2) and both were part  
847 of a Cryogenian sedimentary basin. The layers are tectonically parallel, however,  
848 there are important discrepancies between these two groups here studied, including:  
849 (i) the Itremo Group quartzites represent a more mature sedimentary protolith, also  
850 reflected on the round detrital zircons, while the plagioclase-biotite paragneiss  
851 protoliths represent feldspar-rich, immature sediments with sub- to euhedral detrital

852 zircon grains. (ii) The detrital zircon data implies a major change of source. (iii) The  
853 absence of metamorphic zircon rims on the plagioclase-biotite paragneiss suggests  
854 that it either came from distinct crustal levels and was juxtaposed during collision or  
855 the distinct original composition favoured the zircon growth.

856

### 857 **5.3. Tectonic evolution of the Cryogenian continental sedimentary** 858 **basin**

859 The sample here presented deposited in a Cryogenian (<710 Ma) continental  
860 basin that developed coeval with the late stages of the Imorona-Itsindro Suite, its  
861 major source (population 860–750 Ma from sample DA13-030 – Figs. 6 and 11). We  
862 propose here that this Cryogenian late-magmatic unit can be either correlated with  
863 the Manampotsy group (in the contact between Masora and Antananarivo domains–  
864 Fig.1b) or the Benato formation (in the Anoyesen domain – Fig 1b), implying that this  
865 basin late-Imorona-Itsindro magmatic suite could have been much wider. In addition,  
866 based on mineral composition, well-preserved plagioclase grains, and the absence  
867 of K-feldspar we propose that the source was andesitic in composition. The  
868 Archaean/Palaeoproterozoic zircon cores, within the Tonian-aged igneous crystals  
869 (Fig. 6 and 7), indicate that the source for the Imorona-Itsindro Suite was most likely  
870 the basement of the Antananarivo Domain. The Hf isotopic evidence also supports  
871 this correlation. A minor detrital population of ca. 1.0 to 0.9 Ga zircon in sample DA13-  
872 030 (Fig. 11) could be derived from the Dabolava Arc rocks that crop out to the west,  
873 although the Hf detrital data indicate that this population is less juvenile (Fig. 1b and  
874 2). These crystals are not xenocrysts within the ca. 860–710 Ma igneous zircons, but  
875 detrital zircon with a single age. The predominant late-Tonian-aged detrital zircon,

876 the spatial relation with Imorona-Itsindro Suite and the ca. 2.8–1.7 Ga xenocrysts  
877 support that this sample was deposited in a basin that developed coevally to the  
878 Imorona-Itsindro magmatic event, with some contribution from the Ikalamavony  
879 domain, attesting that both Antananarivo and Ikalamavony domains were attached  
880 by ca. 850 Ma (Figs. 11 and 12).

881 We present three models of Late Tonian-Early Cryogenian tectonic setting for  
882 the sedimentary basin recorded by sample DA-13-030 (Fig. 12). These tectonic  
883 models are based on previous work and the interpretation of our new data, in order  
884 to constraint the tectonic setting for the deposition of this Cryogenian basin. The two  
885 first alternatives encompass subduction zones which magmatic arc is represented by  
886 the Imorona-Itsindro suite.

887 The first model postulates that the Imorona-Itsindro Suite formed in a  
888 continental arc related to a west-dipping subduction zone as proposed by several  
889 authors (BGS-USGS-GLW, 2008; Collins, 2006; Collins and Pisarevsky, 2005;  
890 Collins and Windley, 2002; Kröner et al., 2000). In this case, the sources for pre-  
891 Neoproterozoic detrital zircon grains would be the Antananarivo Domain (including  
892 the Itremo Group), since the “Indian” sources (Masora and Antongil) were distal and  
893 separated by an ocean (Fig. 12a).

894 The second scenario would be the eastward subduction of oceanic crust  
895 (Handke et al., 1999; Boger et al., 2014), and emplacement of the Imorona-Itsindro  
896 Suite also as a continental magmatic arc. In such a circumstance, the Antananarivo  
897 and the Antongil-Masora Domains would be connected to the Dhawar Craton  
898 corroborating to the suggestion that the major source for the older detrital zircons  
899 would be the “Indian” blocks (Fig. 12b). This is supported by the similarities between

900 the Manampotsy metasedimentary sequence and the unit represented here by  
901 sample DA-13-030.

902 The third model envisaged is modified from Tucker et al. (2011b) proposal of  
903 an intracontinental setting with a period of crustal extension. According to these  
904 authors, the Imorona-Itsindro Suite and its related sedimentary rocks are the product  
905 of continental extension (Fig. 12c). The pre-Neoproterozoic sources for the detrital  
906 zircon would mostly be the “Indian” and “Malagasy” blocks, which is a similar situation  
907 to the model of the east-dipping subduction (Fig. 12b). Nevertheless, there is no  
908 evidence of rift sequences related to this tectonic environment (Collins et al. 2003a).  
909 The Cryogenian biotite-plagioclase paragneiss is interpreted as a psammitic rock  
910 with well-preserved plagioclase clasts indicates a fast sedimentation rate, more likely  
911 represented by an orogenic setting.

912 An intriguing chapter in the Neoproterozoic tectonic evolution of central  
913 Madagascar is the paucity of geological units, structures and ages throughout the  
914 Cryogenian period (ca. 720–635 Ma). If we consider the subduction models, there  
915 should be an explanation for the long period of tectonic quiescence and paucity of  
916 magmatic arc activity (Imorona-Itsindro Suite) before the well-documented  
917 continental collision at ca. 550 Ma. The two subduction model alternatives (Fig. 12a  
918 and 12b) do not explain the tectonic quiescence of the Cryogenian (ca. 720–635 Ma),  
919 between the Tonian widespread magmatic activity and the major Ediacaran-  
920 Cambrian continental collision, registered in the samples of this study and in the  
921 overall literature of the Antananarivo and Ikalamavony domains.

922 The two first tectonic scenarios pointed out would need to stall for ca. 100 m.y.  
923 (Fig. 12). That is why we suggest here that the third alternative does not exclude a  
924 prior subduction. In this case, this scenario is proposed for after 710 Ma and could



925 be a consequence for the subduction stall of either tectonic settings (a) and (b). The  
926 tectonic setting for a Cryogenian basin would be an extensional intracontinental  
927 context late-Imorona Itsindro Suite. The corresponding rift related sequences are  
928 absent from the record, which is expected if it is considered that a continental  
929 collisional event took place later at 550 Ma. Major uplift and crustal thickness related  
930 to the Gondwana amalgamation would contribute to the erosion of pre-orogenic  
931 upper crustal units.

932         The tectonic environment of the Great Basin of the western US, for example,  
933 configures a middle to late Cenozoic extension (more than 60 m.y.) of an Archaean  
934 and Palaeoproterozoic continental crust, which involved an initial intra-arc to back  
935 arc deformation and later a transtensional torsion of the continental block inland from  
936 the evolving San Andreas transform system (Dickinson, 2006). This wide rift system  
937 is a product of the interaction between the subduction of ridge-transform systems  
938 that affects the thermal gradients beneath the upper lithospheric mantle (Dickinson,  
939 2006). The continental extension hypothesis for the Tonian tectonic evolution in  
940 central Madagascar, proposed by Tucker et al. (2011b), partially shown in our model  
941 3 (Fig. 12c), could be compared to this recent environment, if it is considered that  
942 there was a previous subduction.

943         We envisage that the Tonian-Cryogenian magmatism and its associated  
944 sedimentary basins might be related to a continental extension due to an outboard  
945 subduction system, partially jammed due to the subduction of a ridge-transform  
946 system. This would be coherent also with the subsequent tectonic quiescence of ca.  
947 100 m.y that preceded the final continental collision. This alternative could be related  
948 to subduction stall between Androyen and Anosyen domains or among the Masora  
949 craton and the Antananarivo domain (Fig.12c). Therefore, either alternative (a) or (b)

950 from figure 12 could evolve to alternative (c). This would differ from the original  
951 purpose of Tucker et al. (2011b), that presumes no subduction at this time.

952 If we consider the western US setting as an analogue, the development of a  
953 transform continental setting would resolve the tectonic Cryogenian paucity. Other  
954 Gondwana-forming belts do have magmatic provinces that are either related to  
955 subduction or intracontinental rifting in the period between ca. 850-750 Ma, such as  
956 the Kaoko belt (Goscombe and Gray 2007, Konopasek et al., 2017), the Ribeira belt  
957 (Meira et al., 2015; Schmitt et al., 2016) or the Arabian Nubian Shield (Johnson et al.  
958 2011). Other orogens have well-documented magmatism related with sedimentary  
959 rift sequences in the same period, like the Damara belt (Miller et al., 2009;  
960 Nascimento et al., 2016).

961 The advance of the converging pre-Gondwana blocks finally collide at ca.  
962 560–520 Ma deforming most central Madagascar lithostratigraphic units. This would  
963 be triggered by an outboard subduction setting, probably related to the SW terranes  
964 of Madagascar, especially the Vohibory Domain (Fig. 1b), and/or the juvenile arc  
965 terranes of eastern Africa including the Tanzanian Ntaka Terrane (Mole et al. 2018)  
966 and the Cabo Delgado Terrane of Mozambique (Bingen et al. 2009). These late  
967 Ediacaran to early Cambrian pervasive multi-phase ductile structures and high-grade  
968 metamorphism collisional event affected most of the Malagasy terranes (Collins,  
969 2006; Tucker et al., 2011b; Armistead et al., 2020). The tectonic pile, preserved in  
970 the studied area, intercalated units of distinct tectonic pre-collisional settings (e.g.  
971 Itremo and Ikalavony Groups; Fig. 3). In addition, the detrital zircon grains from  
972 the three quartzite samples show thick metamorphic rims of ca. 550 Ma (Fig. 8). The  
973 event coincided with widespread magmatism at ca. 540 Ma (Ambalavao Suite), which  
974 marked the terminal Gondwana amalgamation (Fig. 1a; Schmitt et al., 2018).

975

976 **6 - Conclusions**

977 The data presented here reinforce a hypothesis that the tectonic pile of  
978 metasedimentary units from the Itremo-Ikalamavony Domain in central Madagascar  
979 records two distinct basins in time and environment. The lower sequence comprises  
980 quartzite and calc-silicate units with a major Palaeoproterozoic source and a minor  
981 Archaean contribution with a maximum depositional age of ca. 1.78 Ga, based on U–  
982 Pb detrital zircon data. This sequence reflects stable shelf sedimentation on the  
983 basement and or the margins of the Antananarivo Domain and is correlated with the  
984 Itremo Group. The sources are varied and detritus could be derived from either the  
985 eastern cratons (Dharwar, Antongil, Masora) or the western craton (Tanzania). The  
986 abundant near-depositional-age Palaeoproterozoic detritus were likely sourced from  
987 eastern Africa. Our data support an originally contiguous late Palaeoproterozoic to  
988 early Mesoproterozoic sedimentary basin that blanketed central Madagascar, and  
989 possibly included eastern Africa.

990 The upper sequence is a metasedimentary unit represented mostly by biotite-  
991 plagioclase paragneiss, with psammitic protolith, interleaved with  
992 volcanic/subvolcanic andesitic/rhyolitic dykes/sills/flows. The predominant Tonian-  
993 Early Cryogenian (ca. 860-710 Ma) detrital zircon population is probably derived from  
994 the Imorona-Itsindro Suite magmatic rocks, with comparable  $\epsilon_{\text{Hf}}(t)$  values and  $T_{\text{DM Hf}}$   
995 model ages. Some Tonian-aged detrital zircon grains preserve Neoproterozoic to  
996 Palaeoproterozoic cores interpreted as xenocrysts, reinforcing the continental nature  
997 of the Imorona-Itsindro magmatism. This is supported by Hf isotopic data that indicate  
998 an evolved, crustal signature.

999 Our preferred tectonic scenario for this Early Cryogenian sedimentary basin  
1000 would be a continental back arc setting associated with an outboard subduction  
1001 system, which became locked-up by the subduction of a ridge-transform system. We  
1002 suggest that Holocene North America is a modern analogue. We envisage that  
1003 extension was triggered by distal subduction to the west, represented by the Vohibory  
1004 Domain of SW Madagascar and corollaries in eastern Africa. The apparent period of  
1005 tectonic quiescence in central Madagascar between ca. 720 and 635 Ma is explained  
1006 in this model by the conversion of this subduction margin into a transform margin.  
1007 This still enables the oblique approach of Neoproterozoic India with Madagascar and  
1008 Africa to collide in the Ediacaran-Cambrian (Collins and Pisarevsky 2005; Merdith et  
1009 al. 2017) deforming central Madagascar and documented here by ca. 550 Ma zircon  
1010 metamorphic rims in the Itremo Group quartzites.

## 1012 **Acknowledgments**

1013 Authors acknowledge the careful review of Steven Boger and an anonymous  
1014 reviewer. R.S. Schmitt acknowledges the CNPq Grant 311748/2018-0. ASC  
1015 acknowledges Australian Research Council grant FT120100340. We would like to  
1016 thank the undergraduate geology student Luan Dias for helping draft the figures. The  
1017 Razafinjoelina family, in particular Auguste and Berthieu are thanked for providing  
1018 transportation and assistance in the field. The fieldwork was supported by  
1019 Petrobras/CENPES through the Gondwana cooperation project with UFRJ. This  
1020 paper is a contribution to IGCP-628 “The Gondwana geological Map and the tectonic  
1021 evolution of Gondwana” and IGCP 648 “Supercontinent Cycles and Global  
1022 Geodynamics”.

1023

1024           **REFERENCES**

- 1025   Alessio, B.L., Collins, A.S., Siegfried, P.R., Glorie, S., De Waele, B., Payne, J.,  
1026       Archibald, D.B., 2019. Neoproterozoic tectonic geography of the south-east  
1027       Congo Craton in Zambia as deduced from the age and composition of detrital  
1028       zircons. *Geoscience Frontiers*, 10, 2045-2061.
- 1029   Archibald, D.B., Collins, A.S., Foden, J.D., Payne, J.L., Taylor, R., Holden, P.,  
1030       Razakamanana, T., Clark, C., 2015. Towards unravelling the Mozambique  
1031       Ocean conundrum using a triumvirate of zircon isotopic proxies on the  
1032       Ambatolampy Group, central Madagascar. *Tectonophysics* 662, 167-182.
- 1033   Archibald, D.B., Collins, A.S., Foden, J.D., Payne, J.L., Holden, P., Razakamanana,  
1034       T., De Waele, B., Thomas, R.J., Pitfield, P.E.J., 2016. Genesis of the Tonian  
1035       Imorona–Itsindro magmatic Suite in central Madagascar: Insights from U–Pb,  
1036       oxygen and hafnium isotopes in zircon. *Precambrian Research* 281, 312-337.
- 1037   Archibald, D.B., Collins, A.S., Foden, J.D., Razakamanana, T., 2017. Tonian arc  
1038       magmatism in central Madagascar: the petrogenesis of the Imorona-Itsindro  
1039       Suite. *The Journal of Geology* 125(3), 271-297.
- 1040   Archibald, D.B., Collins, A.S., Foden, J.D., Payne, J.L., Macey, P.H., Holden, P.,  
1041       Razakamanana, T., 2018. Stenian-Tonian arc magmatism in west central  
1042       Madagascar: The Genesis of the Dabolava Suite. *Journal of the Geological*  
1043       *Society* 175, 111-129.
- 1044   Archibald, D.B., Collins, A.S., Foden, J.D., Payne, J.L., Holden, P. and  
1045       Razakamanana, T., 2019. Late syn- to post-collisional magmatism in  
1046       Madagascar: The genesis of the Ambalavao and Maevarano Suites.  
1047       *Geoscience Frontiers*, 10, 2063-2084.

- 1048 Armistead, S.E., Collins, A.S., Payne, J.L., Foden, J.D., De Waele, B., Shaji, E.,  
1049 Santosh, M. 2018. A re-evaluation of the Kumta Suture in western peninsular  
1050 India and its extension into Madagascar. *Journal of Asian Earth Sciences* 157,  
1051 317-328.
- 1052 Armistead, S.E., Collins, A.S., Payne, J.L., Cox, G.M., Merdith, A.S., Foden, J.D.,  
1053 Razakamanana, T., De Waele, B. 2019. Evolving marginal terranes during the  
1054 Neoproterozoic supercontinent reorganisation: constraints from the Bemarivo  
1055 Belt in northern Madagascar. *Tectonics* 38, 2019–2035.
- 1056 Armistead, S.E., Collins, A.S., Redaa, A., Gilbert, S., Jepson, G., Gillespie, J.,  
1057 Blades, M.L., Foden, J.D., Razakamanana, T., 2020. Structural Evolution and  
1058 Medium-Temperature Thermochronology of Central Madagascar: Implications  
1059 for Gondwana Amalgamation. *Journal of the Geological Society, London* 177,  
1060 784–798.
- 1061 Armistead, S.E., Collins, A.S., Schmitt, R.S., Costa, R.L., De Waele, B.,  
1062 Razakamanana, T., Payne, J.L., Foden, J.D. in review. Proterozoic basin  
1063 evolution and tectonic geography of Madagascar during the Nuna/Columbia  
1064 Supercontinent. *Tectonics*.
- 1065 Ashwal, L.D., Tucker, R.D., Zinner, E.K., 1999. Slow cooling of deep crustal  
1066 granulites and Pb-loss in zircon. *Geochimica et Cosmochimica Acta* 63, 2839-  
1067 2851.
- 1068 Bauer, W., Walsh, G.J., de Waele, B., Thomas, R.J., Horstwood, M.S.A., Bracciali,  
1069 L., Schofield, D.I., Wollenberg, U., Lidke, D.J., Rasaona, I.T. and Rabarimanana,  
1070 M.H., 2011. Cover sequences at the northern margin of the Antongil Craton, NE  
1071 Madagascar. *Precambrian Research* 189(3-4), 292-312.

- 1072 BGS-USGS-GLW, 2008. Revision de la cartographie geologique et miniere des  
1073 zones Nord, Centre, et Centre Est de Madagascar. BGS Report CR/08/078  
1074 (Keyworth England).
- 1075 Bingen, B., Jacobs, J., Viola, G., Henderson, H.C., Skåra, Ø, Boyd, R., Thomas, R.J.,  
1076 Solli, A., Key, R.M., Daud, E.X.F., 2009. Geochronology of the Precambrian  
1077 crust in the Mozambique belt in NE Mozambique, and implications for Gondwana  
1078 assembly. *Precambrian Research* 170, 231-255.
- 1079 Boger, S.D., Hirdes, W., Ferreira, C.A.M., Schulte, B., Jenett, T., Fanning, C.M.,  
1080 2014. From passive margin to volcano-sedimentary forearc: the Tonian to  
1081 Cryogenian evolution of the Anosy Domain of southeastern Madagascar.  
1082 *Precambrian Research* 247, 159-186.
- 1083 Boger, S.D., Hirdes, W., Ferreira, C.A.M., Jenett, T., Dallwig, R., Fanning, C.M.,  
1084 2015. The 580–520 Ma Gondwana suture of Madagascar and its continuation  
1085 into Antarctica and Africa. *Gondwana Research* 28(3), 1048-1060.
- 1086 Boger, S.D., Maas, R., Pastuhov, M., Macey, P.H., Hirdes, W., Schulte, B., Fanning,  
1087 C.M., Ferreira, C.A.M., Jenett, T., Dallwig, R., 2019. The tectonic domains of  
1088 southern and western Madagascar. *Precambrian Research*, 327: 144-175.
- 1089 Bouvier, A., Vervoort, J.D., Patchett, P.J., 2008. The Lu–Hf and Sm–Nd isotopic  
1090 composition of CHUR: Constraints from unequilibrated chondrites and  
1091 implications for the bulk composition of terrestrial planets. *Earth and Planetary  
1092 Science Letters* 273(1-2), 48-57.
- 1093 Cenki-Tok, B., Berger, A. and Gueydan, F., 2015. Formation and preservation of  
1094 biotite-rich microdomains in high-temperature rocks from the Antananarivo  
1095 Block, Madagascar. *International Journal of Earth Sciences* 105(5), 1471-1483.



- 1096 CGS, 2009a. Map Explanation of 1:100 000 scale (Zone E) Sheets I46 – Ambararata,  
1097 J46 – Beopoaka, I47 – Itondy, J47 – Belobaka, K47 – Ambatofotsy, I48 –  
1098 Miandrivazo, J48 – Betrondro, K48 – Ambatondradama, I49 – Ankotrofotsy, J49  
1099 – Dabolava, K49 – Anjoma-Ramartina, L49 – Vasiana, M49 – Ankazomiriotra,  
1100 N49 – Antsirabe. P.H. Macey, Miller, J.A., Armstrong, R.A., Bisnath, A., Yibas,  
1101 B., Frost-Killian, S., Chevallier, L., Mukosi, N.C., Cole, J., le Roux, P. and  
1102 Haddon, I.G. Ministère de L’Energie et des Mines - Project de Gouvernance des  
1103 Ressources Minérales, Antananarivo, Madagascar and Council for Geoscience,  
1104 Pretoria, South Africa.
- 1105 CGS, 2009b. Map Explanation of 1:100 000 scale sheets (Zone F) G41 –  
1106 Ambohipaky, H41 – Bevary, G42 – Mangoboky, H42 – Bekodoka, G43 –  
1107 Andolamasa, H43 – Andrafialava and parts of G40 – Ankasakasa, F40 – Saint-  
1108 Andre, F41 – Betsalampy, H40 – Maroboaly-Sud, I40 – Soalala-Sud, I41 –  
1109 Andranomavo, F42 – Marovoay Kely, I42 – Mahabe, F43 – Bebao, F44 –  
1110 Antranogoaika, G44 – Morafeno, I43 – Ampoza, H44- Bemolanga and I44  
1111 Makaraingo. P.H. Macey, Miller, J.A., Armstrong, R.A., Ingram, B.A., Bisnath,  
1112 A., Yibas, B., Frost-Killian, S., Chevallier, L., Finkelstein, J. and Haddon, I.G.  
1113 Ministère de L’Energie et des Mines – Project de Gouvernance des Ressources  
1114 Minérales, Antananarivo, Madagascar and Council for Geoscience, Pretoria,  
1115 South Africa.
- 1116 Collins, A.S., 2006. Madagascar and the amalgamation of Central Gondwana.  
1117 Gondwana Research 9, 3-16.
- 1118 Collins, A.S., Pisarevsky, S.A., 2005. Amalgamating eastern Gondwana: The  
1119 evolution of the Circum-Indian Orogens. Earth Science 71, 229-270.

- 1120 Collins, A.S., Windley, B.F., 2002. The tectonic evolution of central and northern  
1121 Madagascar and its place in the final assembly of Gondwana. *The Journal of*  
1122 *geology* 110, 325-339.
- 1123 Collins, A.S., Razakamanana, T., Windley, B.F., 2000. Neoproterozoic extensional  
1124 detachment in central Madagascar: Implications for the collapse of the East  
1125 African Orogen. *Geological Magazine* 137(1), 39-51.
- 1126 Collins, A.S., Windley, B.F., Kröner, A., Fitzsimons, I., Hulscher, B., 2001. The  
1127 Tectonic Architecture of Central Madagascar: Implication on the Evolution of the  
1128 East African Orogeny. *Gondwana Research* 4, 152-153.
- 1129 Collins, A.S., Fitzsimons, I.C.W., Hulscher, B. and Razakamanana, T., 2003a.  
1130 Structure of the eastern margin of the East African Orogen in central  
1131 Madagascar. *Precambrian Research* 123, 111-133.
- 1132 Collins, A.S., Kröner, A., Fitzsimons, I.C.W. and Razakamanana, T. 2003b. Detrital  
1133 Footprint of the Mozambique Ocean: U/Pb SHRIMP and Pb Evaporation Zircon  
1134 Geochronology of Metasedimentary Gneisses in Eastern Madagascar.  
1135 *Tectonophysics*. 375, 77-99.
- 1136 Collins, A.S., Johnson, S., Fitzsimons, I.C.W., Powell, C.McA., Hulscher, B., Abello,  
1137 J. and Razakamanana, T. 2003c. Neoproterozoic deformation in central  
1138 Madagascar: a structural section through part of the East African Orogen. In:  
1139 Proterozoic East Gondwana: Supercontinent Assembly and Breakup (eds.  
1140 Yoshida, M., Windley, B.F. and Dasgupta S.). Geological Society, London,  
1141 Special Publication, 206, 363-379.
- 1142 Collins, A.S., Clark, C., Santosh, M., Sajeev, K., Kropinski, L., McKenzie, S., Hand,  
1143 P.M., Kinny, P.D., 2006. The Mozambique ocean suture in southern India: Age

- 1144 and significance of granulites in the Palghat-Cauvery shear zone system. ASEG  
1145 Extended Abstracts 1, 1-3.
- 1146 Collins, A.S., Kinny, P.D., Razakamanana, T., 2012. Depositional age, provenance  
1147 and metamorphic age of metasedimentary rocks from southern Madagascar.  
1148 Gondwana Research 21(2-3), 353-361.
- 1149 Collins, A.S., Patranabis-Deb, S., Alexander, E., Bertram, C.N., Falster, G.M., Gore,  
1150 R.J., Mackintosh, J., Dhang, P.C., Saha, D., Payne, J.L., Jourdan, F., Backé, G.,  
1151 Halverson, G.P., Wade, B.P., 2015. Detrital mineral age, radiogenic isotopic  
1152 stratigraphy and tectonic significance of the Cuddapah Basin, India. Gondwana  
1153 Research 28(4), 1294-1309.
- 1154 Cox, R., Armstrong, R.A., Ashwal, L.D., 1998. Sedimentology, geochronology and  
1155 provenance of the Proterozoic Itremo Group, central Madagascar, and  
1156 implications for pre-Gondwana palaeogeography. Journal of the Geological  
1157 Society 155(6), 1009-1024.
- 1158 Cox, R., Coleman, D.S., Wooden, J.L., DeOreo, S.B., 2001. A newly recognised Late  
1159 Neoproterozoic metasedimentary sequence in Central Madagascar suggests  
1160 terrane juxtaposition at  $560\pm 7$  Ma during Gondwana assembly, in: Geological  
1161 Society of America Abstracts with Programs 33, A436.
- 1162 Cox, R., Coleman, D.S., Chokel, C.B., DeOreo, S.B., Wooden, J.L., Collins, A.S., De  
1163 Waele, B., Kröner, A., 2004a. Proterozoic tectonostratigraphy and  
1164 paleogeography of Central Madagascar derived from detrital zircon U-Pb age  
1165 populations. The Journal of Geology 112, 379-399.
- 1166 Cox, R., Fernandez, A., Schreurs, G., 2004b. Discussion on tectonic evolution of the  
1167 Proterozoic Itremo Group metasediments in Central Madagascar. Special

- 1168 Publication 206, 2003, 381-399. *Journal of the Geological Society* 161(3), 539-  
1169 541.
- 1170 De Waele, B., Horstwood, M.S.A., Bauer, W., Key, R.M., Pitfield, P.E.J., Potter, C.J.,  
1171 Rabarimana, M., Rafahatelo, J.-M., Ralison, V., Randriamananjara, T., Smith,  
1172 R.A., Thomas, R.J. & Tucker, R.D., 2008. U-Pb detrital zircon geochronological  
1173 provenance patterns of supracrustal successions in central and northern  
1174 Madagascar. *Colloquium of African Geology, Hammamat, Tunisia*, pp. 3.
- 1175 De Waele, B., Fitzsimons, I.C.W., Wingate, M.T.D., Tembo, F., Mapani, B. and  
1176 Belousova, E.A., 2009. The geochronological framework of the Irumide Belt: A  
1177 prolonged crustal history along the margin of the Bangweulu Craton. *American*  
1178 *Journal of Science*, 309(2): 132-187.
- 1179 De Waele, B., Thomas, R.J., Macey, P.H., Horstwood, M.S.A., Tucker, R.D., Pitfield,  
1180 P.E.J., Schofield, D.I., Goodenough, K.M., Bauer, W., Key, R.M., Potter, C.J.,  
1181 Armstrong, R.A., Miller, J.A., Randriamananjara, T., Ralison, V., Rafahatelo,  
1182 J.M., Rabarimanana, M., Bejoma, M., 2011. Provenance and tectonic  
1183 significance of the Palaeoproterozoic metasedimentary successions of central  
1184 and northern Madagascar. *Precambrian Research* 189, 18-42.
- 1185 de Wit, M.J., Bowring, S.A., Ashwal, L.D., Randrianasolo, L.G., Morel, V.P.I.,  
1186 Rambeloson, R.A., 2001. Age and tectonic evolution of Neoproterozoic ductile  
1187 shearzones in southwestern Madagascar, with implications for Gondwana  
1188 studies. *Tectonics* 20, 1-45.
- 1189 Dhuime, B., Hawkesworth, C. and Cawood, P., 2011. When continents formed.  
1190 *Science*, 331(6014): 154-155.
- 1191 Dickinson, W.R., 2006. Geotectonic evolution of the Great Basin. *Geosphere* 2(7),

- 1192 353-368.
- 1193 Emmel, B., Jöns, N., Kröner, A., Jacobs, J., Wartho, J.-A., Schenk, V.,  
1194 Razakamanana, T., Austegard, A., 2008. From closure of the Mozambique  
1195 Ocean to Gondwana break-up: new evidence from geochronological data of the  
1196 Vohibory terrane, southwest Madagascar. *The Journal of Geology* 116, 21-38.
- 1197 Fernandez, A., Schreurs, G., 2003. Tectonic evolution of the Proterozoic Itremo  
1198 Group metasediments in central Madagascar. Geological Society, London,  
1199 Special Publications 206(1), 381-399.
- 1200 Fitzsimons, I.C.W., Hulscher, B., 2005. Out of Africa: detrital zircon provenance of  
1201 central Madagascar and Neoproterozoic terrane transfer across the  
1202 Mozambique Ocean. *Terra Nova* 17(3), 224-235.
- 1203 GAF-BGR, 2008a. Final report. Explanatory notes for the Anosy Domain southeast  
1204 Madagascar. Réalisation des travaux de cartographie géologique de  
1205 Madagascar, révision approfondie de la cartographie géologique et minière aux  
1206 échelles 1/100,000 et 1/500,000 zone Sud. République de Madagascar,  
1207 Ministère de L'énergie et des Mines (MEM/SG/DG/UCP/PGRM), 93 pp.
- 1208 GAF-BGR, 2008b. Final report. Explanatory notes for the Androyen Domain southern  
1209 Madagascar. Réalisation des travaux de cartographie géologique de  
1210 Madagascar, révision approfondie de la cartographie géologique et minière aux  
1211 échelles 1/100,000 et 1/500,000 zone Sud. République de Madagascar,  
1212 Ministère de L'énergie et des Mines (MEM/SG/DG/UCP/PGRM), 81 pp.
- 1213 GAF-BGR, 2008c. Final report. Explanatory notes for the Vohibory Domain  
1214 southwest Madagascar. Réalisation des travaux de cartographie géologique de  
1215 Madagascar, révision approfondie de la cartographie géologique et minière aux

- 1216 échelles 1/100,000 et 1/500,000 zone Sud. Republique de Madagascar,  
1217 Ministère de L'énergie et des Mines (MEM/SG/DG/UCP/PGRM), 85 pp.
- 1218 Glorie, S., De Grave, J., Singh, T., Payne, J.L., Collins, A.S., 2014. Crustal root of  
1219 the Eastern Dharwar Craton: zircon U–Pb age and Lu–Hf isotopic evolution of  
1220 the East Salem Block, southeast India. *Precambrian Research* 249, 229-246.
- 1221 Goncalves, P., Nicollet, C., Montel, J.M., 2004. Petrology and *in situ* U–Th–Pb  
1222 Monazite Geochronology of Ultrahigh-Temperature Metamorphism from the  
1223 Andriamena Mafic Unit, North–Central Madagascar. Significance of a  
1224 Petrographical *P–T* Path in a Polymetamorphic Context, *Journal of Petrology*,  
1225 45, 1923–1957.
- 1226 Goodenough, K.M., Thomas, R.J., De Waele, B., Key, R.M., Schofield, D.I., Bauer,  
1227 W., Tucker, R.D., Rafahatelo, J.-M., Rabarimanana, M., Ralison, A.V,  
1228 Randriamananjara, T., 2010. Post-collisional magmatism in the central East  
1229 African Orogen: The Maevarano Suite of north Madagascar. *Lithos* 116, 18-34.
- 1230 Goscombe, B., Gray, D.R., 2007. The Coastal Terrane of the Kaoko Belt, Namibia:  
1231 Outboard arc-terrane and tectonic significance. *Precambrian Research* 155(1-  
1232 2), 139-158.
- 1233 Grantham, G.H., Manhiça, A.D., Armstrong, R. A., Kruger, F.J., Loubser, M. 2011.  
1234 New SHRIMP, Rb/Sr and Sm/Nd isotope and whole rock chemical data from  
1235 central Mozambique and western Dronning Maud Land, Antarctica: Implications  
1236 for the nature of the eastern margin of the Kalahari Craton and the amalgamation  
1237 of Gondwana. *Journal of African Earth Sciences* 59, 74-100.
- 1238 Griffin, W.L., Wang, X., Jackson, S.E., Pearson, N.J., O'Reilly, S.Y., Xu, X., Zhou, X.,  
1239 2002. Zircon chemistry and magma mixing, SE China: In-situ analysis of Hf

- 1240 isotopes, Tonglu and Pingtan igneous complexes. *Lithos* 61, 237–269.
- 1241 Griffin, W L; Powell, W.J.; O'Reilly, S.Y., 2008. GLITTER : Data reduction software  
1242 for laser ablation ICP-MS. *Laser Ablation ICP-MS in the Earth Sciences: Current*  
1243 *practices and outstanding issues*, 308-311.
- 1244 Handke, M.J., Tucker, R.D., Ashwal, L.D., 1999. Neoproterozoic continental arc  
1245 magmatism in west-central Madagascar. *Geology* 27, 351-354.
- 1246 Horton, F., Hacker, B., Kylander-Clark, A., Holder, R., Jöns, N., 2016. Focused  
1247 radiogenic heating of middle crust caused ultrahigh temperatures in southern  
1248 Madagascar. *Tectonics* 35, 293-314.
- 1249 Jackson, S.E., Pearson, N.J., Griffin, W.L., Belousova, E.A., 2004. The application  
1250 of laser ablation-inductively coupled plasma-mass spectrometry to in situ U–Pb  
1251 zircon geochronology. *Chemical Geology* 211(1-2), 47-69.
- 1252 Jacobs, J., Fanning, C.M., Henjes-Kunst, F., Olesch, M., Paech, H., 1998.  
1253 Continuation of the Mozambique Belt into East Antarctica: Grenville-Age  
1254 Metamorphism and Polyphase Pan-African High-Grade Events in Central  
1255 Dronning Maud Land. *Journal of Geology* 106, 385-406.
- 1256 Jacobs, J., Thomas, R. J. 2004. Himalayan-type indenter-escape tectonics model for  
1257 the southern part of the late Neoproterozoic–early Paleozoic East African–  
1258 Antarctic orogen. *Geology* 32, 721-724.
- 1259 Johnson, P.R., Andresen, A., Collins, A.S., Fowler, A.R., Fritz, H., Ghebreab, W.,  
1260 Kusky, T., Stern, R.J., 2011. Late Cryogenian-Ediacaran history of the Arabian-  
1261 Nubian Shield: A review of depositional, plutonic, structural, and tectonic events  
1262 in the closing stages of the northern East African Orogen. *Journal of African*  
1263 *Earth Sciences*. 61, 167-232.

- 1264 Jöns, N., Schenk, V., 2008. Relics of the Mozambique Ocean in the central East  
1265 African Orogen: evidence from the Vohibory Block of southern Madagascar.  
1266 *Journal of Metamorphic Geology* 26, 17-28.
- 1267 Jöns, N., Schenk, V., 2011. The ultrahigh temperature granulites of southern  
1268 Madagascar in a polymetamorphic context: implications for the amalgamation of  
1269 the Gondwana supercontinent. *European Journal of Mineralogy* 23, 127-156.
- 1270 Kabete, J., Groves, D., McNaughton, N., Dunphy, J., 2006. The geology, SHRIMP  
1271 U–Pb geochronology and metallogenic significance of the Ankisatra-Besakay  
1272 District, Andriamena belt, northern Madagascar. *Journal of African Earth  
1273 Sciences* 45(1), 87-122.
- 1274 Key, R.M., Pitfield, P.E.J., Thomas, R.J., Goodenough, K.M., De Waele, B.,  
1275 Schofield, D.I., Bauer, W., Horstwood, M.S.A., Styles, M.T., Conrad, J.,  
1276 Encarnacion, J., Lidke, D.J., O'Connor, E.A., Potter, C., Smith, R.A., Walsh,  
1277 G.J., Ralison, A.V., Randriamananjara, T., Rafahatelo, J.-M., and  
1278 Rabarimanana, M., 2011. Polyphase Neoproterozoic orogenesis within the East  
1279 Africa–Antarctica Orogenic Belt in central and northern Madagascar. *Geological  
1280 Society, London, Special Publications* 357(1), 49-68.
- 1281 Konopásek, J., Hoffmann, K-H., Sláma, J., Kosler, J., 2017. The onset of flysch  
1282 sedimentation in the Kaoko Belt (NW Namibia) – Implications for the pre-  
1283 collisional evolution of the Kaoko-Dom Feliciano-Gariep orogen. *Precambrian  
1284 Research* 298, 220-234.
- 1285 Kröner, A., Windley, B.F., Jaeckel, P., Brewer, T.S., Razakamanana, T., 1999.  
1286 Precambrian granites, gneisses and granulites from Madagascar: new zircon  
1287 ages and regional significance for the evolution of the Pan-African orogen.



- 1288 Journal of the Geological Society (London) 156, 1125-1135.
- 1289 Kröner, A., Hegner, E., Collins, A.S., Windley, B.F., Brewer, T.S., Razakamanana,  
1290 T., Pidgeon, R.T., 2000. Age and magmatic history of the Antananarivo Block,  
1291 central Madagascar, as derived from zircon geochronology and Nd isotopic  
1292 systematics. American Journal of Science 300(4), 251-288.
- 1293 Küster, D., Utke, A., Leupolt, L., Lenoir, J.L., Haider, A., 1990. Pan-African granitoid  
1294 magmatism in northeastern and southern Somalia. Berliner  
1295 Geowissenschaftliche Abhandlungen 120, 519-536.
- 1296 Lancaster, P.J., Dey, S., Storey, C.D., Mitra, A., Bhunia, R.K., 2015. Contrasting  
1297 crustal evolution processes in the Dharwar craton: insights from detrital zircon  
1298 U–Pb and Hf isotopes. Gondwana Research 28(4), 1361-1372.
- 1299 Lenoir, J.-L., Küster, D., Liégeois, J.-P., Utke, A., Haider, A., Matheis, G., 1994.  
1300 Origin and regional significance of late Precambrian and early Palaeozoic  
1301 granitoids in the Pan-African belt of Somalia. Geologische Rundschau 83, 624-  
1302 641.
- 1303 Ludwig, K.R., 2012. User's Manual for Isoplot 3.75. A Geochronological Toolkit for  
1304 Microsoft Excel.
- 1305 Maibam, B., Gerdes, A., Goswami, J. N., 2016. U–Pb and Hf isotope records in  
1306 detrital and magmatic zircon from eastern and western Dharwar craton, southern  
1307 India: Evidence for coeval Archaean crustal evolution. Precambrian Research  
1308 275, 496-512.
- 1309 McMillan, A., Harris, N.B.W., Holness, M., Ashwal, L., Kelley, S., Rambeloson, R.,  
1310 2003. A granite-gabbro complex from Madagascar: constraints on melting of the  
1311 lower crust. Contributions to Mineralogy and Petrology 145(5), 585-599.

- 1312 Meira, V.T., Garcia-Casco, A., Juliani, C., Almeida, R.P., Schorscher, J.H.D., 2015.  
1313 The role of intracontinental deformation in supercontinent assembly: insights  
1314 from the Ribeira Belt, Southeastern Brazil (Neoproterozoic West Gondwana).  
1315 *Terra Nova* 27(3), 206-217.
- 1316 Merdith, A. S., Collins, A. S., Williams, S. E., Pisarevsky, S., Foden, J. D., Archibald,  
1317 D. B., Blades, M.L., Alessio, B., Armstead, S., Plavsa, D., Clark, C., Müller, R.D.,  
1318 2017. A full-plate global reconstruction of the Neoproterozoic. *Gondwana*  
1319 *Research* 50, 84-134.
- 1320 Miller, R. M. G., Frimmel, H. E., Halverson, G. P., 2009. Passive continental margin  
1321 evolution. Neoproterozoic to Early Palaeozoic evolution of Southwestern Africa.  
1322 In: Gaucher, C., Sial, A.N., Halverson, G.P., Frimmel, H.E. (Eds.),  
1323 Neoproterozoic-Cambrian Tectonics, Global Change and Evolution: A Focus on  
1324 Southwestern Gondwana. *Developments in Precambrian Geology* 16. Elsevier,  
1325 pp. 161-181.
- 1326 Mohan, M.R., Sarma, D.S., McNaughton, N.J., Fletcher, I.R., Wilde, S.A., Siddiqui,  
1327 M.A., Rasmussen, B., Krapez, B., Gregory, C.J., Kamo, S.L., 2014. SHRIMP  
1328 zircon and titanite U-Pb ages, Lu-Hf isotope signatures and geochemical  
1329 constraints for ~2.56 Ga granitic magmatism in Western Dharwar Craton,  
1330 Southern India: Evidence for short-lived Neoproterozoic episodic crustal growth?.  
1331 *Precambrian Research*, 243, 197-220.
- 1332 Mole, D.R., Barnes, S.J., Taylor, R.J.M., Kinny, P.D., Fritz, H., 2018. A relic of the  
1333 Mozambique Ocean in south-east Tanzania. *Precambrian Research*, 305, 386-  
1334 426.
- 1335 Nascimento, D.B., Ribeiro, A., Trouw, R.A.J., Schmitt, R.S., Passchier, C.W., 2016.

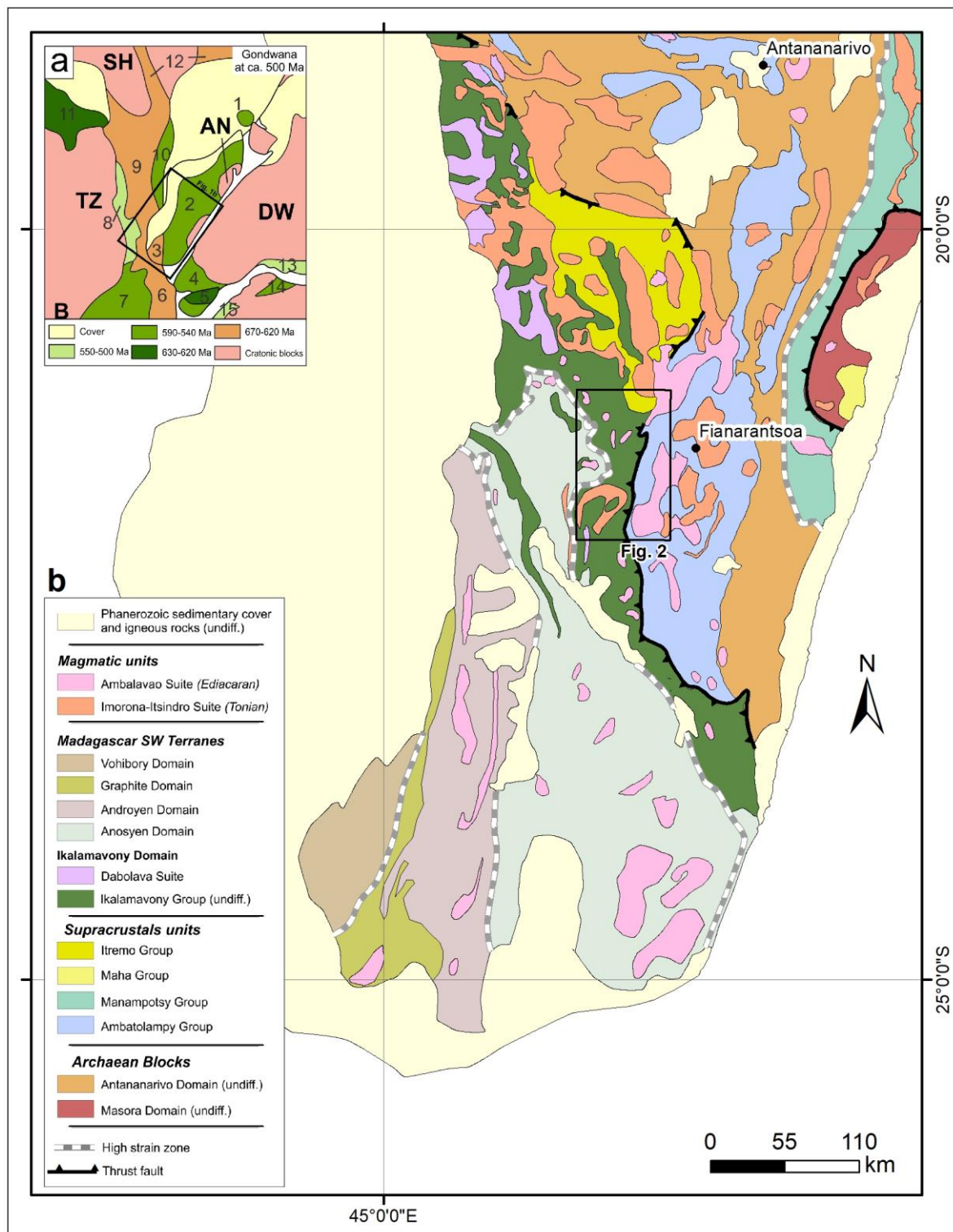
- 1336 Stratigraphy of the Neoproterozoic Damara Sequence in northwest Namibia:  
1337 Slope to basin sub-marine mass-transport deposits and olistolith fields.  
1338 Precambrian Research 278, 108-125.
- 1339 Paquette, J.-L., Nédélec, A., 1998. A new insight into Pan-African tectonics in the  
1340 East–West Gondwana collision zone by U–Pb zircon dating of granites from  
1341 central Madagascar. Earth and Planetary Science Letters 155(1-2), 45-56.
- 1342 Praveen, M.N., Santosh, M., Yang, Q.Y., Zhang, Z.C., Huang, H., Singaneni, S.,  
1343 Sajinkumar, K.S., 2014. Zircon U–Pb geochronology and Hf isotope of felsic  
1344 volcanics from Attappadi, southern India: implications for Neoproterozoic  
1345 convergent margin tectonics. Gondwana Research 26(3-4), 907-924.
- 1346 Reddy, S.M., Collins, A.S. and Mruma, A. 2003. Complex High-Strain Deformation in  
1347 the Usagaran Orogen, Tanzania: Structural Setting of Palaeoproterozoic  
1348 Eclogites. Tectonophysics. 375, 101-123.
- 1349 Roig, J.Y.; Tucker, R.D.; Delor, C.; Peters, S.G. and Théveniaut, H., 2012. Carte  
1350 Géologique de la République de Madagascar à 1/1,000,000. Ministère des  
1351 Mines, PGRM, Antananarivo, République Madagascar 1.
- 1352 Sarma, D.S., McNaughton, N.J., Belusova, E., Mohan, M.R., Fletcher, I.R., 2012.  
1353 Detrital zircon U–Pb ages and Hf-isotope systematics from the Gadag  
1354 Greenstone Belt: Archean crustal growth in the western Dharwar Craton, India.  
1355 Gondwana Research 22, 843–854.
- 1356 Scherer, E.; Munker, C.; Mezger, K., 2001. Calibration of the Lutetium-Hafnium  
1357 Clock. Science 293(5536), 1766-1766.
- 1358 Schmitt, R.S., Fragoso, R.A., Collins, A.S., 2018. Suturing Gondwana in the  
1359 Cambrian: The Orogenic Events of the Final Amalgamation. In: Siegesmund, S.,

- 1360 Basei, M.A.S., Oyhantçabal, P., Oriolo, S. (Eds.), *Geology of Southwest*  
1361 *Gondwana*. Springer International Publishing, pp. 411-432.
- 1362 Schmitt, R.S., Trouw, R.A.J., Schmus, W.R.V., Armstrong, R., Stanton, N.S.G., 2016.  
1363 The tectonic significance of the Cabo Frio Tectonic Domain in the SE Brazilian  
1364 margin: a Paleoproterozoic through Cretaceous saga of a reworked continental  
1365 margin. *Brazilian Journal of Geology* 46, 37-66.
- 1366 Schofield, D.I., Thomas, R.J., Goodenough, K.M., De Waele, B., Pitfield, P.E.J., Key,  
1367 R.M., Bauer, W., Walsh, G.J., Lidke, D.J., Ralison, A.V., Rabarimanana, M.,  
1368 Rafahatelo, J.M., Randriamananjara, T., 2010. Geological evolution of the  
1369 Antongil craton, NE Madagascar. *Precambrian Research* 182(3), 187-203.
- 1370 Sláma, J., Košler, J., Condon, D.J., Crowley, J.L., Gerdes, A., Hanchar, J.M.,  
1371 Horstwood, M.S.A., Morris, G.A., Nasdala, L., Norberg, N., Schaltegger, U.,  
1372 Schoene, B., Tubrett, M.N., Whitehouse, M.J., 2008. Plešovice zircon - A new  
1373 natural reference material for U–Pb and Hf isotopic microanalysis. *Chemical*  
1374 *Geology* 249(1-2), 1-35.
- 1375 Stern, R.J., 1994. Arc assembly and continental collision in the Neoproterozoic East  
1376 African Orogen: Implications for the consolidation of Gondwanaland. *Annual*  
1377 *Review of Earth and Planetary Sciences* 22, 319-351.
- 1378 Stern, R.J., 2002. Crustal evolution in the East African Orogen: A neodymium isotopic  
1379 perspective. *Journal of African Earth Sciences* 34, 109-117.
- 1380 Storey, M., Mahoney, J.J., Saunders, A.D., Duncan, R.A., Kelley, S.P., Coffin, M.F.,  
1381 1995. Timing of hot spot-related volcanism and the breakup of Madagascar and  
1382 India. *Science* 267(5199), 852-855.
- 1383 Teklay, M., Kroner, A., Mezger, K., Oberhansli, R., 1998. *Geochemistry, Pb–Pb*

- 1384 single zircon ages and Nd–Sr isotope composition of Precambrian rocks from  
1385 southern and eastern Ethiopia: implications for crustal evolution in East Africa.  
1386 *Journal of African Earth Sciences* 26, 207- 227.
- 1387 Thomas, R.J., De Waele, B., Schofield, D.I., Goodenough, K.M., Horstwood, M.,  
1388 Tucker, R., Bauer, W., Annells, R., Howard, K., Walsh, G., Rabarimanana, M.,  
1389 Rafahatelo, J.M., Ralison, A.V. and Randriamananajara, T., 2009. Geological  
1390 evolution of the Neoproterozoic Bemarivo Belt, northern Madagascar.  
1391 *Precambrian Research*, 172(3-4): 279-300.
- 1392 Thomas, R.J., Spencer, C., Bushi, A.M., Baglow, N., Boniface, N., de Kock, G.,  
1393 Horstwood, M.S.A., Hollick, L., Jacobs, J., Kajara, S., Kamihanda, G., Key, R.M.,  
1394 Maganga, Z., Mbawala, F., McCourt, W., Momburi, P., Moses, F., Mruma, A.,  
1395 Myambilwa, Y., Roberts, N.M.W., Saidi, H., Nyanda, P., Nyoka, K., Millar, I.,  
1396 2016. Geochronology of the central Tanzania Craton and its southern and  
1397 eastern orogenic margins. *Precambrian Research* 277, 47-67
- 1398 Tucker, R.D., Ashwal, L.D., Handke, M.J., Hamilton, M.A., Le Grange, M.,  
1399 Rambeloson, R.A., 1999. U-Pb geochronology and isotope geochemistry of the  
1400 Archean and Proterozoic rocks of north-central Madagascar. *The Journal of*  
1401 *Geology* 107(2), 135-153.
- 1402 Tucker, R.D., Kusky, T.M., Buchwaldt, R., Handke, M.J., 2007. Neoproterozoic  
1403 nappes and superposed folding of the Itremo Group, west-central Madagascar.  
1404 *Gondwana Research* 12(4), 356-379.
- 1405 Tucker, R.D., Roig, J.Y., Macey, P.H., Delor, C., Amelin, Y., Armstrong, R.A.,  
1406 Rabarimanana, M.H., Ralison, A. V., 2011a. A new geological framework for  
1407 south-central Madagascar, and its relevance to the “out-of-Africa” hypothesis.

- 1408 Precambrian Research 185, 109-130.
- 1409 Tucker, R.D., Roig, J.Y., Delor, C., Amelin, Y., Goncalves, P., Rabarimanana, M.H.,  
1410 R., A.V., Belcher, R.W., 2011b. Neoproterozoic extension in the Greater  
1411 Dharwar Craton: a reevaluation of the “Betsimisaraka suture” in Madagascar.  
1412 Canadian Journal of Earth Sciences 48(2), 389-417.
- 1413 Tucker, R.D., Roig, J.Y., Moine, B., Delor, C., Peters, S.G., 2014. A geological  
1414 synthesis of the Precambrian shield in Madagascar. Journal of African Earth  
1415 Sciences 94, 9-30.
- 1416 Vermeesch, P., 2018. IsoplotR: A free and open toolbox for geochronology.  
1417 Geoscience Frontiers, 9(5), 1479-1493.
- 1418 Whitehouse, M.J., Windley, B.F., Stoesser, D.B., Al-Khirbash, S., Ba-Bttat, M.A.O.,  
1419 Haider, A., 2001. Precambrian basement character of Yemen and correlations  
1420 with Saudi Arabia and Somalia. Precambrian Research 105, 357-369.
- 1421 Woodhead, J., Hergt, J., Shelley, M., Eggins, S., Kemp, R., 2004. Zircon Hf-isotope  
1422 analysis with an excimer laser, depth profiling, ablation of complex geometries,  
1423 and concomitant age estimation. Chemical Geology 209(1-2), 121-135.
- 1424 Yang, Q. Y., Santosh, M., 2015. Zircon U–Pb geochronology and Lu–Hf isotopes  
1425 from the Kolar greenstone belt, Dharwar Craton, India: Implications for crustal  
1426 evolution in an ocean-trench-continent transect. Journal of Asian Earth Sciences  
1427 113, 797-811.
- 1428 Zhou, J.-L., Li, X.-H., Tang, G.-Q., Liu, Y. and Tucker, R.D., 2018. New evidence for  
1429 a continental rift tectonic setting of the Neoproterozoic Imorona-Itsindro Suite  
1430 (central Madagascar). Precambrian Research, 306: 94-111.
- 1431 Zhou, J.-L., Shao, S., Luo, Z.-H., Shao, J.-B., Wu, D.-T. and Rasoamalala, V., 2015.

1432 Geochronology and geochemistry of Cryogenian gabbros from the  
1433 Ambatondrazaka area, east-central Madagascar: Implications for Madagascar-  
1434 India correlation and Rodinia paleogeography. *Precambrian Research*, 256(0):  
1435 256-270.  
1436



1437

1438

1439

1440

1441

1442

1443

1444

1445

1446

1447

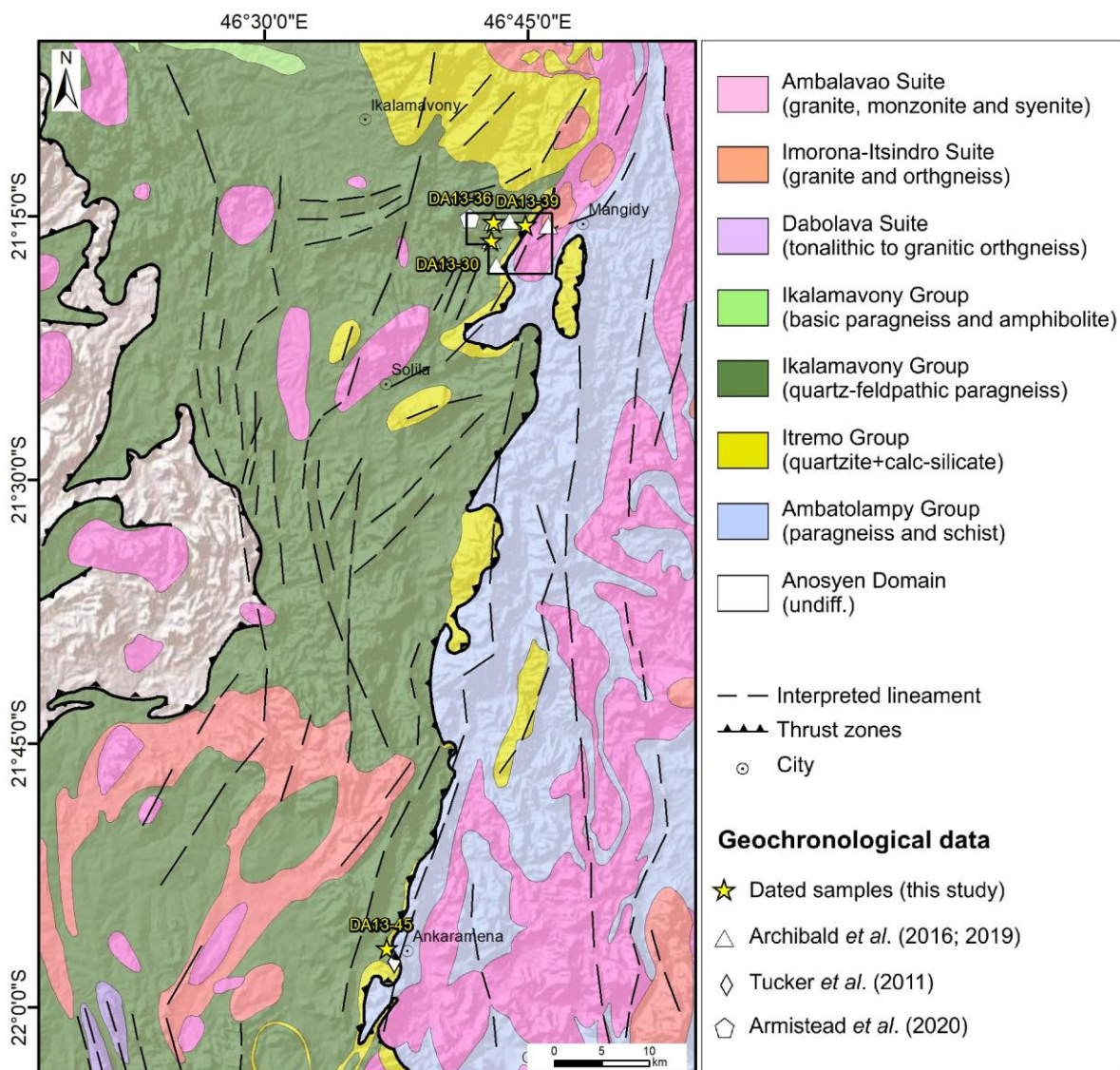
1448

**Figure 1: a)** Gondwana configuration at ca. 500 Ma with pre-Gondwana cratons sutured by Neoproterozoic-Cambrian mobile belts (modified from Schmitt et al., 2018), highlighting central and south Madagascar. Pink polygons show Precambrian cratons, orange and green polygons show different orogenic events according to age intervals. The letters and number on the map represent Gondwana cratons and mobile belts, respectively. Abbreviations: EA=East Antarctica; B=Bangweulu Block; AN=Antogil Domain; DW=Dharwar; SH=Sahara and TZ=Tanzania; Legend key: 1-Seychelles; 2-Madagascar (Bemarivo, Antananarivo, Itremo-Ikalamavony, Androyen and Anosyen); 3-Madagascar (Vohibory); 4-Southern Granulites; 5-Sri Lanka; 6-Eastern Granulite; 7-Zambesi; 8-Western Granulite; 9-Arabian/Nubian Shield (South); 10-Galana (Azania); 11-Oubanguides; 12-Arabian/Nubian Shield (North); 13-Eastern Ghats; 14-Reworked border of the Napier Complex; 15-Prince Olaf Coast/Kemp Land; **b)** Simplified geological map of Central and Southern Madagascar showing the distribution of (volcano)metasedimentary units from Antananarivo and Itremo-Ikalamavony domains, Maha and Manampotsy groups.



1449  
1450

Manampotsy groups and undifferentiated Masora, Anosyen, Androyen and Vohibory domains, Imorona-Itsindro and Ambalavao suites and Phanerozoic undifferentiated rocks (modified from Roig et al., 2012).

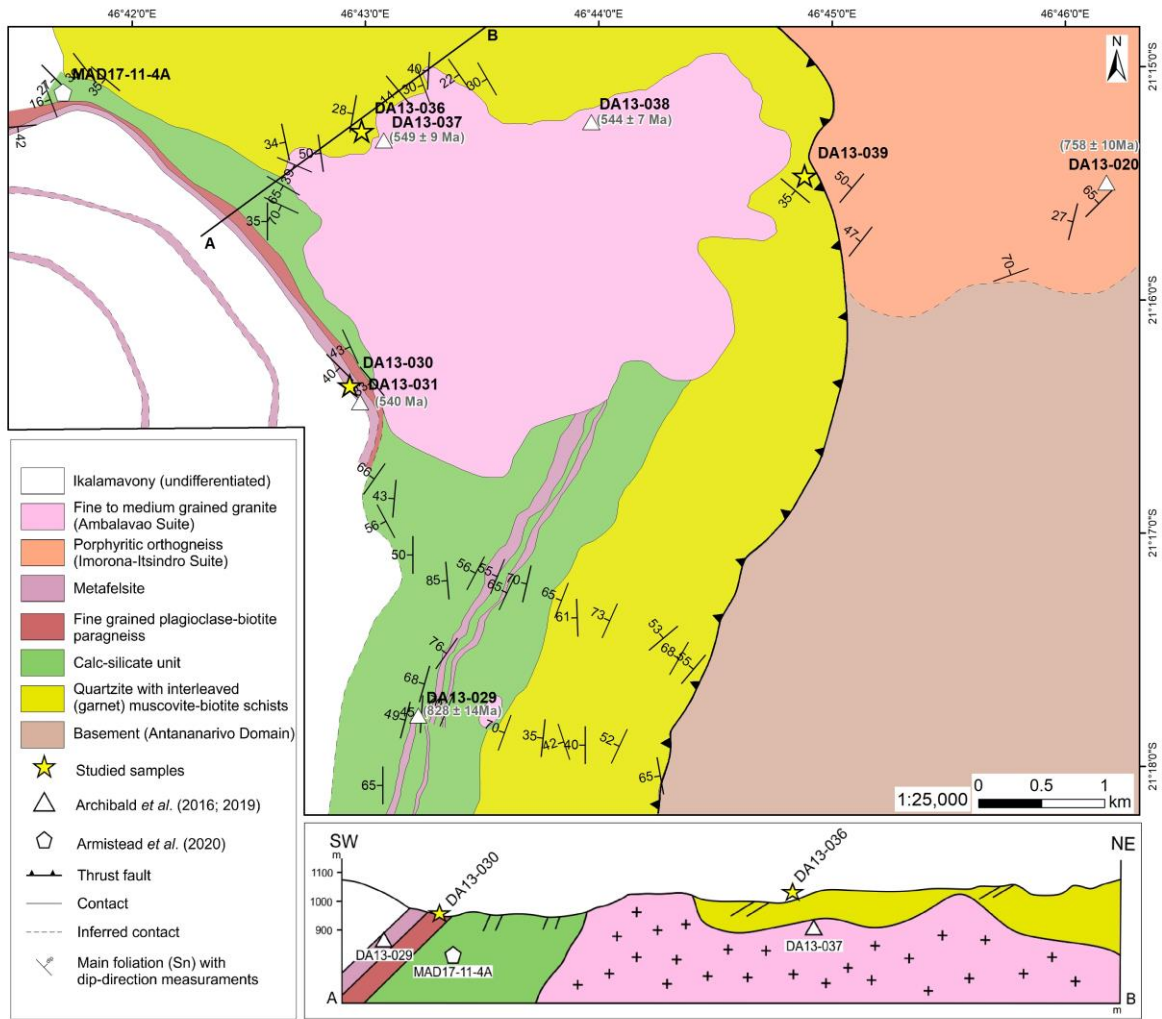


1451  
1452

1453  
1454

**Figure 2:** Geological map of western region of central Madagascar with location of dated samples, shown in figure 1 (modified from Roig et al., 2012). The mapped area is shown in the black polygon.

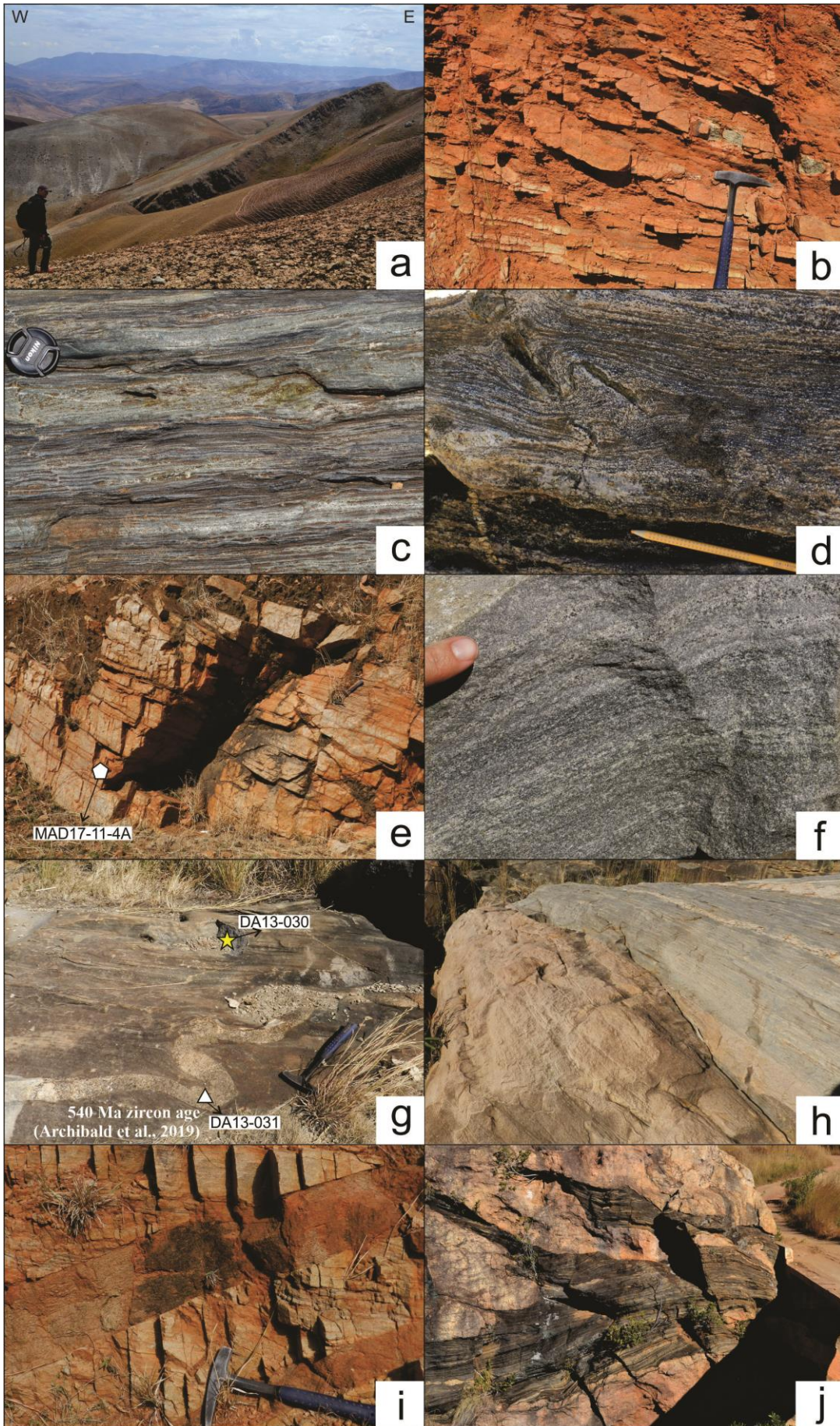
1455



1456  
1457

1458 **Figure 3:** Detailed geological map of the area with measurements of main foliation, sample locations of this  
 1459 study (except DA13-045), and sample location of Archibald et al. (2016, 2019), and other sample, not analyzed.  
 1460 In addition, a SW-NE cross section, not scaled, is presented and the location of the area according to the  
 1461 Figure 2.

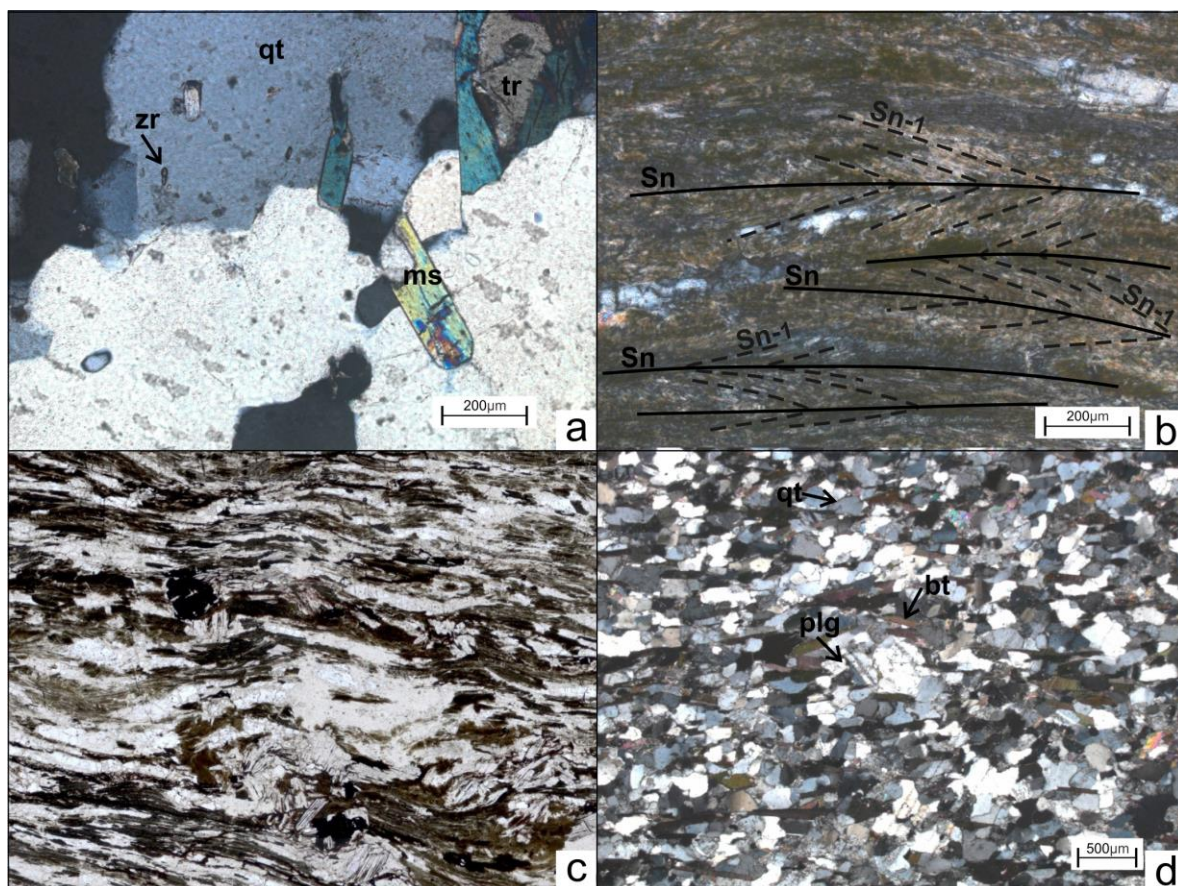
1462



1465  
1466  
1467  
1468  
1469  
1470  
1471  
1472  
1473  
1474

**Figure 4:** **a)** Mountain ranges of the quartzite unit with interlayered (garnet- sillimanite) muscovite-biotite schists. The sedimentary layering is parallel to the tectonic foliation and both dip to west; **b)** Intercalation of quartzite and schist on the upper package of the quartzite unit; **c)** Diopside-gneiss of the bottom of the calc-silicate unit showing mylonitic foliation; **d)** Asymmetric fold in laminated white marble; **e)** Quartzite layer within the calc-silicate unit – note sample MAD17-11-4A – dated by Armstead et al. (in review); **f)** Fine grained homogeneous plagioclase-biotite paragneiss; **g)** Folded granitic dyke cross-cutting the plagioclase-biotite-paragneiss – note samples DA13-031 and DA13-030; dated by D.B. Archibald unpublished and our study, respectively; **h)** Contact between the plagioclase-biotite paragneiss (grayish on top) and the metafelsite (pinkish on bottom). Note concordant tectonic foliation; **i)** Foliated mafic dykes (granodioritic in composition) that cross-cut the quartzite; **j)** Ambalavao Suite pink granite intruding the calc-silicate sequence.

1475

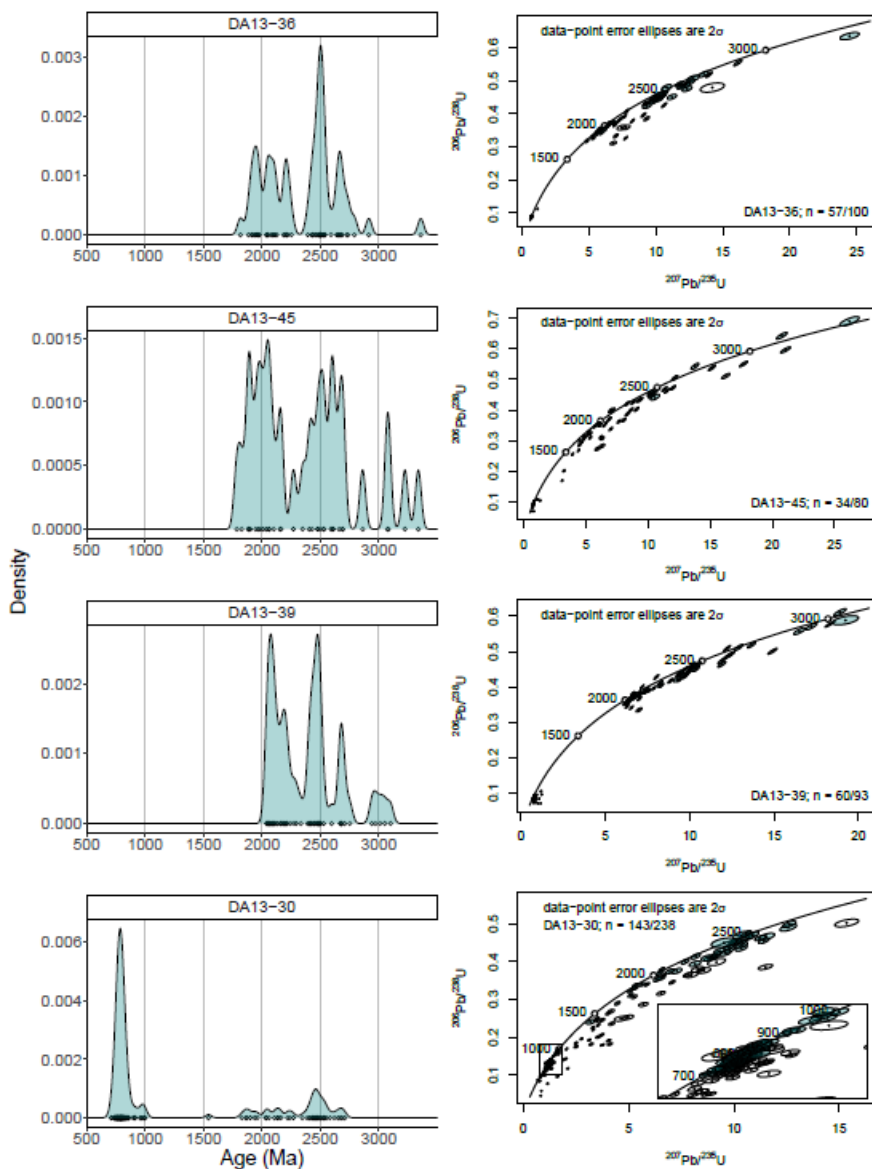


1476  
1477

**Figure 5:** **a)** Photomicrograph of thin layered quartzite near the contact with the calc-silicate unit, showing muscovite, tremolite and zircon, in cross-polarized view; **b)** Cross-polarized view of a (Garnet-sillimanite) muscovite-biotite schist from the quartzite unit with tight chevron folds, showing that the Sn tectonic foliation (axial plane of the micro-folds), measured in the field, corresponds to a second phase of ductile deformation. The folded metamorphic minerals represent an older foliation (Sn-1); **c)** Plane-polarized view of the sillimanite-garnet schist, showing asymmetric micro-folds east-vergent; **d)** Fine grained plagioclase-biotite-paragneiss in thin section. This is sample DA-13-030, dated here.

1478  
1479  
1480  
1481  
1482  
1483  
1484

1485



1486

1487

1488

1489

**Figure 6:** Probability density plots (left) and Concordia (right) diagrams for analyzed detrital zircon grains from samples DA13-036 (a), DA13-045 (b), DA13-039 (c) and DA13-030 (d). Within the Concordia diagram the analysis within 10% of concordance are coloured, and all other analyses are white.

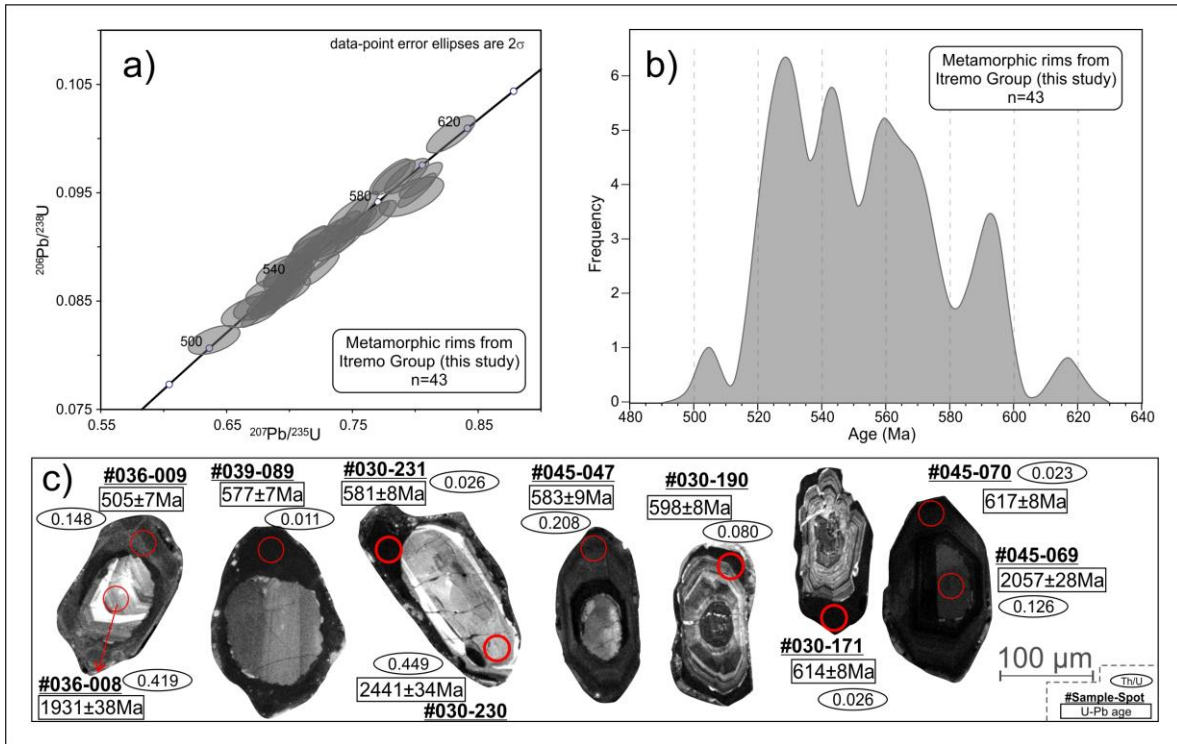


Figure 7: Selected CL images of zircon grains with U-Pb and Lu-Hf analysis spots and Th/U ratios from samples: a) DA13-036 b) DA13-045 c) DA13-039 d) DA13-030.

1490  
1491

1492  
1493

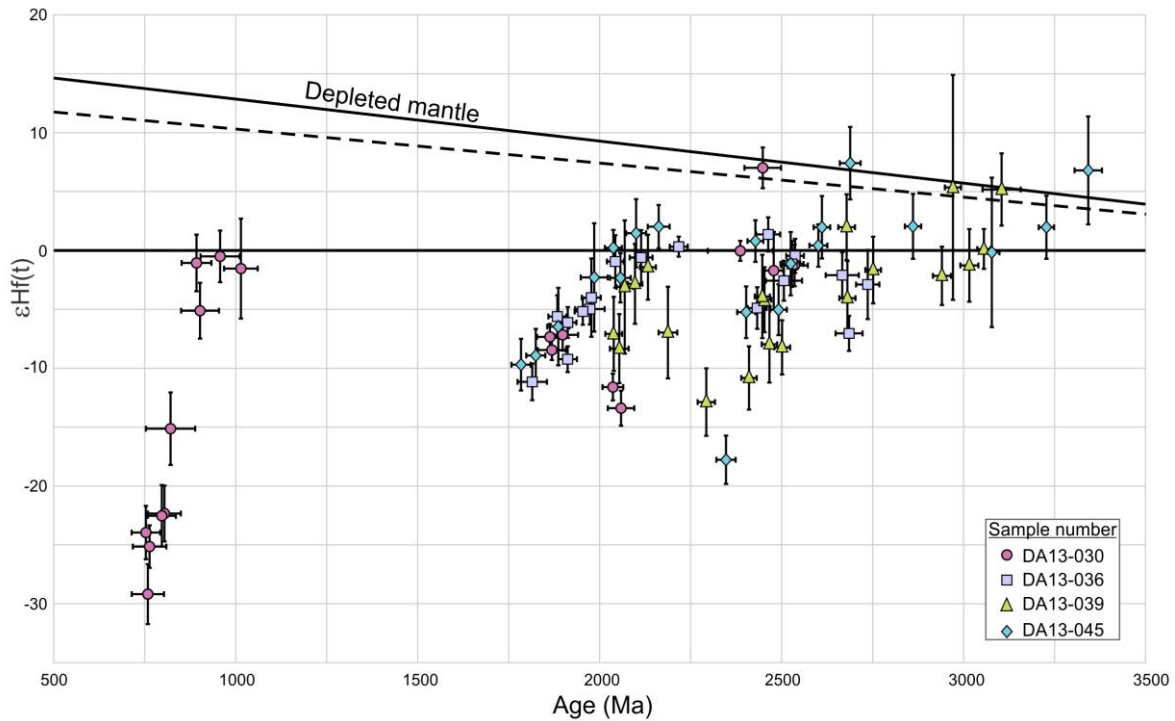
1494



1495  
1496

**Figure 8:** Metamorphic rim data from three quartzite samples. **a)** U-Pb concordia of metamorphic rim data; **b)** histogram diagram with the same data as in (a) and **c)** selected CL images from metamorphic zircon domains showing metamorphic rims with U-Pb ages and Th/U ratios. Data from the sample DA-030 are shown only in Fig. 8c.

1497  
1498  
1499  
1500



1501  
1502

1503

1504  
1505

**Figure 9:** Hf isotopic evolution diagram with data obtained on detrital zircons from the four samples of this study. Error bars are in 2 sigma.

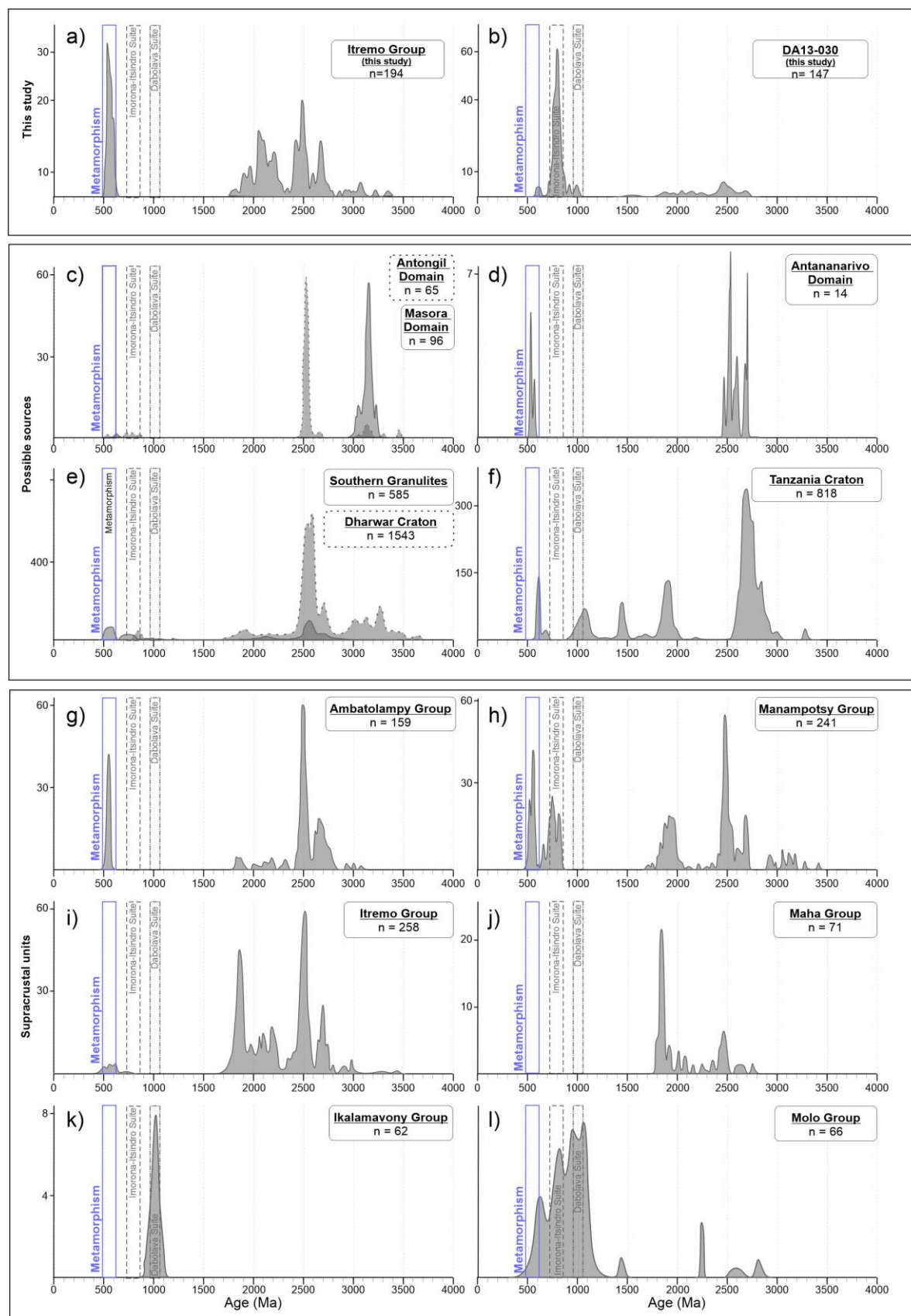


**Figure 10:** Comparative U–Pb age distribution of detrital zircon for supracrustal units in central Madagascar and their possible sources.. **a)** DA13-036, DA13-039 and DA13-045 (this study); **b)** DA13-030 (this study); **c)** Antongil and Masora domains (BGS-USGS-GLW, 2008; Collins et al. 2003; Schofield et al. 2010); **d)** Antananarivo Domain – Betsiboka Suite (BGS-USGS-GLW, 2008); **e)** Dharwar Craton (Collins et al. 2015;

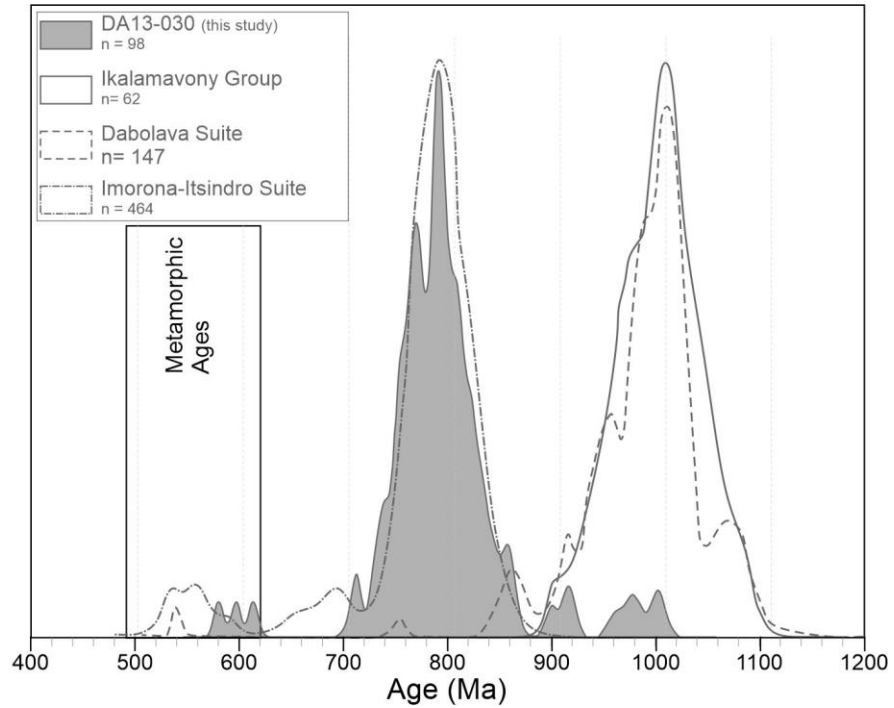
1506  
1507

1508  
1509  
1510  
1511



1512 Glorie et al. 2014; Ishwar-Kumar et al. 2013; Jayananda et al. 2013; Lancaster et al. 2015; Maibam et al. 2016);  
 1513 f) Tanzania Craton (Thomas et al. 2016); g) Ambatolampy Group (Archibald et al. 2015); h) Manampotsy  
 1514 Group (BGS-USGS-GLW, 2008; Tucker et al. 2011a); i) Itremo Group (Cox et al. 1998, 2004; De Waele et al.  
 1515 2011; Fitzimons and Hulscher 2005; Tucker et al. 2011); j) Maha Group (De Waele et al. 2011); k) Ikalamavony  
 1516 Group (Tucker et al. 2011) and l) Molo Group (Cox et al., 2004).

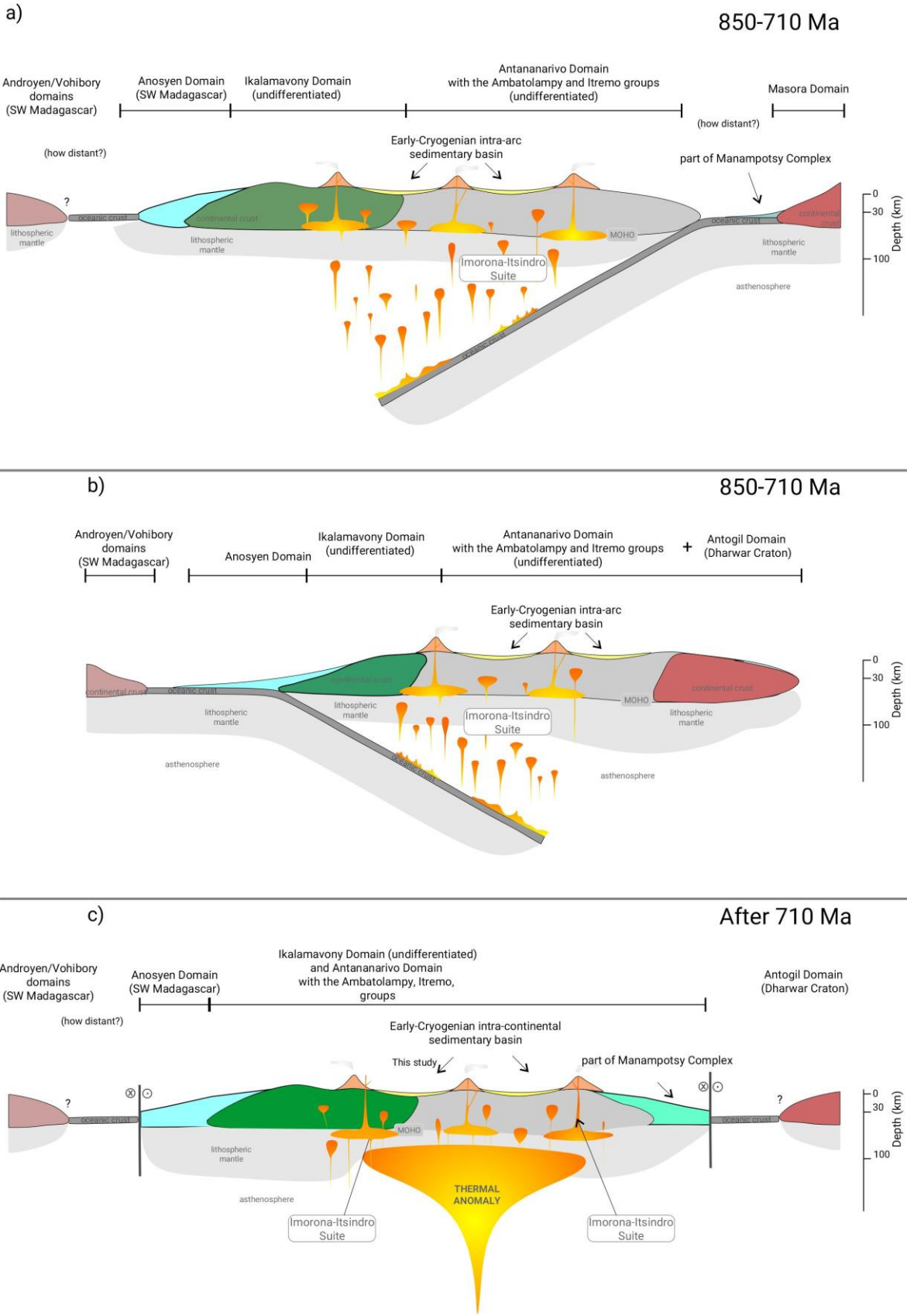
1517



1518

1520 **Figure 11:** Comparative probability and density diagram to identify the possible main source for the population  
 1521 younger than 1.1 Ga, also more abundant, of sample DA13-030. U-Pb zircon data from Ikalamavony Group,  
 1522 Dabolava Suite and Imorona-Itsindro Suite is compiled from Tucker et al. (2011), Archibald et al. (2016, 2018)  
 1523 and BGS-USGS-GLW (2008).

1524



1525  
1526

1527  
1528  
1529  
1530

**Figure 12:** Different tectonic settings for Late Tonian Early Cryogenian interval (850-710 Ma) modified from diverse authors, to envisage the depositional scenario for the basin represented by sample DA13-030 from this study. **a)** West-dipping subduction related to a convergent continental margin between Antananarivo Domain (Madagascar) and Dharwar Craton (India) interpreted by Collins (2006), Key et al. (2011) and Kröner et al.

1531 (2000); **b)** East-dipping subduction and the deposition of supracrustal units from the Anosyen Domain above  
1532 Antananarivo Domain by Boger et al. (2014) and **c)** After 710 Ma an intracontinental setting would prevail late-  
1533 Imorona-Itsindro magmatic activity due to subduction stall (this alternative is a variation of the model by Tucker  
1534 et al., 2011b, 2014).

1535

1536

1537

## FIGURE CAPTIONS

1538 Figure 1: a) Gondwana configuration at ca. 500 Ma with pre-Gondwana  
1539 cratons sutured by Neoproterozoic-Cambrian mobile belts (modified from Schmitt et  
1540 al., 2018), highlighting central and south Madagascar. Pink polygons show  
1541 Precambrian cratons, orange and green polygons show different orogenic events  
1542 according to age intervals. The letters and number on the map represent Gondwana  
1543 cratons and mobile belts, respectively. Abbreviations: EA=East Antarctica;  
1544 B=Bangweulu Block; DW=Dharwar; SH=Sahara and TZ=Tanzania; Legend key: 1-  
1545 Seychelles; 2-Madagascar (Bemarivo, Antananarivo, Itremo-Ikalamavony, Androyen  
1546 and Anosyen); 3-Madagascar (Vohibory); 4-Southern Granulites; 5-Sri Lanka; 6-  
1547 Eastern Granulite; 7-Zambesi; 8-Western Granulite; 9-Arabian/Nubian Shield  
1548 (South); 10-Galana (Azania); 11-Oubanguides; 12-Arabian/Nubian Shield (North);  
1549 13-Eastern Ghats; 14-Reworked border of the Napier Complex; 15-Prince Olaf  
1550 Coast/Kemp Land; b) Simplified geological map of central and southern Madagascar  
1551 showing the distribution of (volcano)metasedimentary units from Antananarivo and  
1552 Itremo-Ikalamavony domains, Maha and Manampotsy groups and undifferentiated  
1553 Masora, Anosyen, Androyen and Vohibory domains, Imorona-Itsindro and  
1554 Ambalavao suites and Phanerozoic undifferentiated rocks (modified from Roig et al.,  
1555 2012).

1556 Figure 2: Geological map of western region of central Madagascar with  
1557 location of dated samples, shown in figure 1 (modified from Roig et al., 2012). The  
1558 area mapped in detail is shown in the black polygon.

1559 Figure 3: Detailed geological map of the area with measurements of main  
1560 foliation, sample locations of this study (except DA13-045), and sample locations of  
1561 Archibald et al. (2016; 2019 and unpublished data), and other samples that were not  
1562 analysed. In addition, a SW-NE cross section, not scaled, is presented and the  
1563 location of the area according to the Figure 2.

1564 Figure 4: a) Mountain ranges of the quartzite unit with interlayered (garnet-  
1565 sillimanite) muscovite-biotite schists. The sedimentary layering is parallel to the  
1566 tectonic foliation and both dip to west; b) Intercalation of quartzite and schist on the  
1567 upper package of the quartzite unit; c) Diopside-gneiss from the bottom of the calc-  
1568 silicate unit showing mylonitic foliation; d) Asymmetric fold in laminated white marble;  
1569 e) Quartzite layer within the calc-silicate unit – note sample MAD17-11-4A – was  
1570 dated by Armstead et al. (unpublished); f) Fine-grained homogeneous plagioclase-  
1571 biotite paragneiss; g) Folded granitic dyke cross-cutting the plagioclase-biotite-  
1572 paragneiss – note samples DA13-031 and DA13-030; dated by D.B. Archibald  
1573 unpublished and our study, respectively; h) Contact between the plagioclase-biotite  
1574 paragneiss (grayish on top) and the metafelsite (pinkish on bottom). Note concordant  
1575 tectonic foliation; i) Foliated mafic dykes that cross-cut the quartzite; j) Ambalavao  
1576 Suite pink granite intruding the calc-silicate sequence.

1577 Figure 5: a) Photomicrograph of thin layered quartzite near the contact with  
1578 the calc-silicate unit, showing quartz (qt), muscovite (ms), tremolite (tr) and zircon  
1579 (zr), in cross-polarized view; b) Cross-polarized view of a (Garnet-sillimanite)  
1580 muscovite-biotite schist from the quartzitic unit with tight chevron folds, showing that

1581 the Sn tectonic foliation (axial plane of the micro-folds), measured in the field,  
1582 corresponds to a second phase of ductile deformation. The folded metamorphic  
1583 minerals represent an older foliation (Sn-1); c) Plane-polarized view of the sillimanite-  
1584 garnet schist, showing asymmetric micro-folds east-vergent; d) Photomicrograph of  
1585 fine-grained plagioclase-biotite-paragneiss in thin section, showing quartz (qt),  
1586 plagioclase (plg) and biotite (bt). This is sample DA-13-030, dated here.

1587 Figure 6: Probability density plots (left) and Concordia (right) diagrams for  
1588 analysed detrital zircon grains for samples DA13-036 (a), DA13-045 (b), DA13-039  
1589 (c) and DA13-030 (d).

1590 Figure 7: Selected CL images of zircon grains with U-Pb and Lu-Hf analysis  
1591 spots and Th/U ratios from samples: a) DA13-036 b) DA13-045 c) DA13-039 d)  
1592 DA13-030.

1593 Figure 8: Metamorphic rim data from zircon in the three quartzite samples. a)  
1594 U-Pb concordia diagram; b) probability density diagram with the same data as in (a)  
1595 and c) selected CL images from metamorphic zircon domains showing metamorphic  
1596 rims with U-Pb ages and Th/U ratios. Data from the sample DA-030 is shown only in  
1597 fig. 8c.

1598 Figure 9: Hf isotopic evolution diagram with data obtained on detrital zircons  
1599 from the four samples of this study. Error bars are in 2 sigmas. In addition to CHUR,  
1600 the evolution of depleted-mantle (Griffin et al., 2002) and the evolution curve for new  
1601 crust derived from the upper-mantle (Dhuime et al., 2011) are shown.

1602 Figure 10: Comparative U-Pb age distribution of detrital zircon for supracrustal  
1603 units in central Madagascar and their possible sources. Yellow bars show the main  
1604 intervals – described in item 4.1. a) DA13-036, DA13-039 and DA13-045 (this study);

1605 b) DA13-030 (this study); c) Antongil and Masora domains (BGS-USGS-GLW, 2008;  
1606 Collins et al. 2003; Schofield et al. 2010); d) Antananarivo Domain – Betsiboka Suite  
1607 (BGS-USGS-GLW, 2008; Tucker et al., 1999; Kröner et al., 2000); e) Dharwar Craton  
1608 (Collins et al. 2015; Glorie et al. 2014; Ishwar-Kumar et al. 2013; Jayananda et al.  
1609 2013; Lancaster et al. 2015; Maibam et al. 2016); f) Tanzania Craton (Thomas et al.  
1610 2016); g) Ambatolampy Group (Archibald et al. 2015); h) Manampotsy Group (BGS-  
1611 USGS-GLW, 2008; Tucker et al. 2011a); i) Itremo Group (Cox et al. 1998, 2004; De  
1612 Waele et al. 2011; Fitzimons and Hulscher 2005; Tucker et al. 2011); j) Maha Group  
1613 (De Waele et al. 2011); k) Ikalamavony Group (Tucker et al. 2011) and l) Molo Group  
1614 (Cox et al., 2004).

1615 Figure 11: Comparative probability density diagram to identify the possible  
1616 main source for sample DA13-030. U-Pb zircon data from Ikalamavony Group,  
1617 Dabolava Suite and Imorona-Itsindro Suite are compiled from Tucker et al. (2011),  
1618 Archibald et al. (2016, 2018) and BGS-USGS-GLW (2008).

1619 Figure 12: Different tectonic settings for Late Tonian to Early Cryogenian  
1620 interval (ca. 850-710 Ma) modified from diverse authors, to envisage the depositional  
1621 scenario for the basin represented by sample DA13-030 from this study. a) West-  
1622 dipping subduction related to a convergent continental margin between Antananarivo  
1623 Domain (Madagascar) and Dharwar Craton (India) interpreted by Collins (2006), Key  
1624 et al. (2011) and Kröner et al. (2000); b) East-dipping subduction and the deposition  
1625 of supracrustal units from the Anosyen Domain above the Antananarivo Domain as  
1626 suggested by Boger et al. (2014) and c) After 710 Ma an intracontinental setting  
1627 would prevail late to the Imorona-Itsindro magmatic activity due to subduction stall  
1628 (this alternative is a variation of the model by Tucker et al., 2011b, 2014).

1629 **LIST OF SUPPLEMENTARY TABLES**

1630 Supplementary table 1: U-Pb data of detrital zircons from samples DA13-036,  
1631 DA13-045, DA13-039 and DA13-030 (LA-ICP-MS)

1632 Supplementary table 2: Lu-Hf data of detrital zircons from samples DA13-030,  
1633 DA13-036, DA13-039 and DA13-045 (LA-ICP-MS)